ADDIS ABABA UNIVERSITY

NATURAL AND COMPUTATIONAL SCIENCE

DEPARTMENT OF CHEMISTRY

Computational Investigation of $Ca(OH)_2$ / CaO for Thermochemical Energy Storage

By

Sada Husen Abarago

Advisor

Dr. Getachew Gizaw

Prof. Ahimed Mustefa

June, 2014

Computational Investigation of $Ca(OH)_2$/CaO for Thermochemical Energy Storage

Sada Husen Abarago

A Thesis Submitted to

The Department of Chemistry

Presented in Partial Fulfillment of the Requirement for the Degree of Master of Science in Chemistry (Physical Chemistry)

Addis Ababa University

Addis Ababa, Ethiopia

June 2024

ADDIS ABABA UNIVERSITY

NATURAL AND COMPUTATIONAL SCIENCES

DEPARTMENT OF CHEMISTRY

This is to certify that the thesis prepared by Sada Husen Abarago, entitled: ‘‘Computational investigation of $Ca(OH)_2$/CaO for thermochemical energy storage’’ and submitted in partial fulfillment of the requirements of the Degree of Master of Science in Chemistry (Physical Chemistry) compiles with regulations of the University and meets the accepted standards with respect to originality and quality.

Signed by the Examining Committee:

Examiner : _____Signature_____ Date _____

Examiner : _____Signature_____Date _____

Advisor: Dr. Getachew Gizaw ___Signature _____ Date _____

_____

Chair of Department or Graduate Program Coordinator

Abstract

Computational Investigation of $Ca(OH)_2$/CaO for Thermochemical energy storage

Thermochemical energy storage (TCES) systems are essential for improving the efficiency and reliability of renewable energy technologies. Calcium hydroxide ($Ca(OH)_2$) and calcium oxide (CaO) are promising candidates for TCES due to their high energy density and reversible hydration-dehydration reactions. This study presents a comprehensive computational investigation of Li and Li_2-doped $Ca(OH)_2$/CaO clusters using the Vienna Ab initio Simulation Package (VASP) and ABCluster software. Clusters of $Ca(OH)_2$ and CaO with sizes ranging from n=1 to n=10 was prepared, and low-lying isomers were selected for detailed analysis.

Density Functional Theory (DFT) calculations were conducted to optimize the geometries and compute binding energy, formation energy, and second-order energy corrections. It is evident from the stability analysis that the doped clusters' average binding energies and formation energies are higher than those of the comparable pure $Ca(OH)_n$ and (CaO) clusters. Maximum peaks of the second order energy differences are seen for $LiCa_{n-1}(OH)_n$ (n=2−10), $Li_2Ca_{n-1}(OH)_n$ (n=2−10) and $LiCa_{n-1}O_n$ (n=2-10), $Li_2Ca_{n-1}O_n$ (n=2-10) clusters at n=6, 4, and 2 suggesting that these clusters are more stable than the clusters that are surrounding them. Clusters with n=6 were specifically chosen for evaluating energy storage potential. Additionally, dehydration curves were plotted to assess the energy release characteristics.

The results demonstrate that Li and Li_2 doping significantly enhances the thermochemical properties of $Ca(OH)_2$/CaO clusters, resulting in higher energy storage density, improved reaction kinetics, and better cycling stability.

Acknowledgements

First of all, I would like to thank Allah, Alhamdulillah, then I would like to express my deepest gratitude to my advisor, Dr. Getachew Gizaw, for his invaluable guidance, support, and encouragement throughout the course of my research. His insightful advice, patience, and unwavering commitment to my academic growth have been instrumental in the completion of this thesis. I am truly fortunate to have had the opportunity to work under his mentorship.

I would also like to thank my brother, Mohamed Husen, for his generous funding and ongoing encouragement. His faith in my ability and consistent drive have been a source of strength for me throughout difficult times. Mohamed's tolerance and understanding, as well as his willingness to help me financially, have been crucial.

I am profoundly thankful to my friends Salahadin Mustefa, Sabir Faris, Miftah Nasir, Mohamed Ahimed, and Woliyi Mohamed for their financial support and steadfast friendship. Your generosity has allowed me to concentrate on my studies without the worry of financial strain.

Finally, I would like to thank my family, other friends, and colleagues who have provided me with the necessary encouragement and understanding throughout this journey. Your support has been a pillar of strength for me.

Thank you all for your contributions to my academic journey. This thesis would not have been possible without your support.

Table of contents

List of figures.....6
Appendix.....7
List of Tables.....8
1. INTRODUCTION.....8
1.2 Objective of Thesis.....9
2. Literature Review.....10
2.1 CaO/Ca(OH)2 Thermochemical Energy Storage.....10
2.2 Effect of Energy Storage Conditions on CaO/Ca(OH)2 TES.....10
2.2.1. Effect of Form of Water in Hydration and Dehydration Atmosphere.....10
2.2.2. Effect of Temperature and Vapor Pressure.....10
2.3 Enhancing the Performance of CaO-Based Materials in CaO/$Ca(OH)_2$ TES.....11
2.3.1 CaO-Based Materials Modified with LiOH in CaO/Ca(OH)2 TES.....11
3. Computational method and model.....12
3.1 Density functional theory (DFT).....12
3.1.1 Formal Development of Density Functional Theory.....12
Kohn-Sham Equations.....13
The Kohn-Sham approach involves solving a set of self-consistent equations for non-interacting electrons in an effective potential. The KS equations are:13
3.4 Ca (OH)2 and CaO cluster preparation Method.....13
4. Result and discussion.....14
4.1a. Geometries of Li(CaOH)n−1On and LiCan-1On(n=2−10) clusters.....15
4.1b. Geometries of Li2(CaOH)n−1On (n=2−10) and Li2Can-1On (n=2−10) clusters.....18
4.1c. Li-i- (CaOH)n and Li-i-(CaO)n (n=2−10) clusters.....20
4.1d. LiNO3 - (CaOH)n (n=1-10).....23
4.1e. LiCl-(Ca(OH)2)n (n=1-10) clusters.....25
4.1f. LiOH- (Ca(OH)2)n (n=1-10).....27
4.2 Energetic Properties.....28

4.2.1 Pure (CaOH)2 /CaO clusters.....28
4.2.2 Li Doped (CaOH)2 /CaO clusters.....30
I. Binding Energy.....30
II. Second Order Energy.....33
Table 2: Second Order Energies of $Ca(OH)_2$ and CaO Clusters (n = 1-10).....36
4.3 Defect energy.....36
4.4 Dehydration Energy of $Ca(OH)_2$ for Thermochemical Energy Storage.....38
4.4.1 Dehydration curve of p[H2O] vs Temperature plot of pure Ca(OH)2/CaO clusters.....39
Conclusion.....41
Reference.....42

List of figures

FIG. 1a. The most stable Isomer geometries for $Li(CaOH)_{n-1}O_n$ clusters. n= 2-10

FIG. 1b. The most stable Isomer geometries for $Li(Ca_{n-1}O_n)$ clusters. n= 2-10

FIG. 2a. The most stable Isomer geometries for $Li_2(CaOH)_{n-1}O_n$ clusters. n= 2-10

FIG. 2b. The most stable Isomer geometries for $Li_2(Ca_{n-1}O_n)$ clusters. n= 2-10

FIG. 3a. The most stable Isomer geometries for Li-i-$((CaOH)_2)_n$ clusters. n= 2-10

FIG. 3b. The most stable Isomer geometries for Li-i-$(CaO)_n$ clusters. n= 2-10

FIG.4 Most stable isomers of LiOH-$Ca(OH)_n$ clusters (n=1-10)

FIG.5 Most stable isomers of LiCl-$(Ca(OH)_2)_n$ (n=1-10) clusters

FIG.6 Most stable isomers of LiOH- $(Ca(OH)_2)_n$ (n=1-10) clusters

Appendix

APPENDIX 1

$Li(Ca_{n-1}OH)_n$ low-lying isomers

APPENDIX 2

$Li_2(Ca_{n-1}OH)_n$ (n=2−10), $Li_2Ca_{n-1}O_n$ (n=2−10) And

Li-i-$Ca(OH)_2$, Li-i-CaO low-lying isomers

APPENDIX 3

$LiNO_3$, LiCl, and LiOH - [$Ca(OH)_2$ low-lying isomers

List of Tables

Table 1. Binding Energy and Formation Energy, of $Ca(OH)_2$ and CaO.
Table 2: Second Order Energies of $Ca(OH)_2$ and CaO Clusters (n = 1-10)
Table 3: Computed Defect Energies of $Ca(OH)_2$ and CaO Clusters Doped with Lithium Atoms

1. INTRODUCTION

Thermochemical energy storage is an important component of thermal energy storage because it addresses the long-term energy storage challenges associated with some renewable energy sources. Using a chemical reaction as a thermochemical energy storage method offers numerous advantages since the chemically stored energy is relatively high and is unaffected by heat losses. [1] There are six categories of materials that are used in TES: inorganic hydroxide, metal hydride, organics, carbonate, ammonia decomposition system, and redox system.[2] Inorganic hydroxides decompose at 523-873 K, making them ideal for storing heat at medium temperatures. The typically utilized inorganic hydroxides include $Ca(OH)_2$/CaO, $Mg(OH)_2$/MgO, $Ba(OH)_2$/BaO, and $Sr(OH)_2$/SrO. [2] Among the various materials for TES, lime has promising features for practical application, i.e., low cost, no waste, non-toxicity, good stability, controllable safety, and high energy density. However, the low heat-storage rate, low conversion, and the poor reversibility of heat storage and heat release cannot satisfy practical demands, arising partially from the low permeability and agglomeration of lime and hydrated lime in the cyclic process of charge and discharge. [7]

The heat-storage principal of lime can be expressed as

$$Ca(OH)_2(s) \leftrightharpoons CaO(s) + H_2O(g) \qquad \Delta H_r = 104.4 \text{ kJ/mol} \qquad (1)$$

It was observed by Shkatulov and colleagues that KNO_3 and $LiNO_3$ can both significantly lower the dehydration temperature and speed up the dehydration of both $Ca(OH)_2$ and $Mg(OH)_2$. [8]

LiOH doping improves the dehydration rate of $Ca(OH)_2$ by lowering its activation energy. [9] The charge and discharge temperatures of the process can theoretically be adjusted over a wide range (about, 300-650 °C). [4] In eq (1) The forward endothermic reaction is known as dehydration, while the reverse exothermic response is hydration. Heat received during dehydration can be stored with an energy density of 1.4 MJ/kg-$Ca(OH)_2$ when calcium oxide and water are separated. Heat is released during hydration. [5] This reaction cycle has been employed for several uses, such as self-heating food containers for hot drinks like coffee, tea, or milk.[6]

The research on thermochemical heat storage is still in its early stages. Preliminary study has focused on hydroxides like CaO/$Ca(OH)_2$ and MgO/$Mg(OH)_2$ for thermochemical heat storage. [20] Darkwa and O'Callaghan (1997) found that a CaO/$Ca(OH)_2$ heat storage system may warm an automobile engine, reducing the release of pollutants during cold boot.

The initial test showed that the interaction between 28 g CaO and 9 g water under 1.5 atm resulted in a temperature rise of 220 1C from ambient temperature.[21] Ogura et al. (2001) used radial fins in the reactor of a $Ca(OH)_2$ thermochemical heat storage device to improve heat exchange.[22]

In this study we generated $Ca(OH)_2$ and CaO cluster of n=(1-10), using ABcluster software and optimized using The Vienna Ab initio Simulation Package (VASP). The low-lying isomer energy, bond distance, bond angle, and other geometry were studied. This study also investigates Li doping of CaO/Ca(OH)2 systems, as well as $Ca(OH)_2$ doping using LiOH, LiCl, and $LiNO_3$. Substituting Li for Ca alters crystal structure and symmetry. The altered crystal structure has an impact on heat storage through thermochemical processes.[20]

1.2 Objective of Thesis

General objective;

The general objective of this work is to design and optimize $Ca(OH)_2$/CaO hydroxide materials for enhanced thermochemical energy storage, focusing on maximizing energy storage efficiency and stability through detailed analysis of their dehydration and rehydration processes through DFT calculations.

Specific objectives:

- Develop accurate computational models of $Ca(OH)_2$ and CaO clusters using ABclusters software.
- Optimize $Ca(OH)_2$ and CaO clusters using VASP to identify and characterize low-lying isomers with potential applications in thermochemical energy storage.
- Calculate the Second order, binding and formation energies of $Ca(OH)_2$ and CaO clusters for varying cluster sizes (n = 1-10) to understand the energetics of these materials.
- Simulate the dehydration process of $Ca(OH)_2$ to CaO, identifying the energy barriers and reaction pathways.

2. Literature Review

2.1 $CaO/Ca(OH)_2$ Thermochemical Energy Storage

$CaO/Ca(OH)_2$ TES is based on the hydration/dehydration reactions of CaO.[26] In the solar dehydrator, the decomposition of $Ca(OH)_2$ produces CaO and water vapor, which are then stored in separate tanks. During this process, heat energy is converted into chemical energy and stored in CaO. When heat is required, CaO and water vapor are transferred from their storage tanks to the hydrator, where they react to release heat.[27] During the heat storage stage, calcium hydroxide absorbs heat and decomposes into calcium oxide and water vapor. In the exothermic stage, calcium oxide is combined with water vapor to form calcium hydroxide. Due to the nature of this reaction, heat can be released at temperatures ranging from room temperature to nearly 500°C under atmospheric pressure. By adjusting the water vapor pressure during the heat storage stage, the temperature can be maintained around 500°C. This makes the $CaO/Ca(OH)_2$ system highly suitable for heat storage applications. Additionally, its low cost and high reaction enthalpy (104.4 kJ/mol) enhance its potential as a promising solution for thermal energy storage.[28]

2.2 Effect of Energy Storage Conditions on $CaO/Ca(OH)_2$ TES

2.2.1. Effect of Form of Water in Hydration and Dehydration Atmosphere

The form of water used in the hydration process significantly affects the performance of CaO-based materials in $CaO/Ca(OH)_2$ thermochemical energy storage (TES) systems. Sakellarious et al. reported that the required dehydration temperature is notably lower when the hydration reaction is carried out using distilled water compared to when it is conducted in pure steam. This indicates that the type of water used can influence the efficiency and temperature requirements of the dehydration process.[29]

2.2.2. Effect of Temperature and Vapor Pressure

Knoll et al. [30] suggested that the hydration temperature of CaO is influenced by the concentration of water vapor. Yan et al. [27] discovered that both the dehydration temperature and the initial temperature of the sample during the hydration reaction affect the performance of CaO-based materials in $CaO/Ca(OH)_2$ thermochemical energy storage (TES) systems, as follows:

a. As the dehydration temperature increased, the dehydration rate (the ratio of dehydration conversion to time) of $Ca(OH)_2$ accelerated, significantly enhancing the dehydration conversion.

b. When the initial sample temperature of the hydration reaction was increased, both the hydration rate (the ratio of hydration conversion to time) and the hydration conversion of CaO decreased sharply.

2.3 Enhancing the Performance of CaO-Based Materials in $CaO/Ca(OH)_2$ TES

Natural CaO-based materials used for thermochemical energy storage often experience significant sintering after numerous hydration and dehydration cycles. This results in reduced reactivity and decreases structural stability of the materials.[31]

Many researchers have found that modification methods can effectively enhance the energy storage performance of CaO-based materials in $CaO/Ca(OH)_2$ thermochemical energy storage systems.

2.3.1 CaO-Based Materials Modified with LiOH in $CaO/Ca(OH)_2$ TES

To analyze the micro-mechanism of CaO-based material modified with LiOH, Yan et al. [20] utilized crystal structure models of quantum chemistry based on the transition state principle and first-principles calculations. The model calculations revealed changes in the molecular structure of the transition state, indicating that the addition of LiOH altered the dehydration kinetics of $Ca(OH)_2$. The energy barrier for the dehydration of $Ca(OH)_2$ decreased from 0.4 to 0.11 eV with the addition of LiOH. This reduction suggests that the dehydration reaction of Li-doped $Ca(OH)_2$ could occur at lower temperatures compared to the original $Ca(OH)_2$.

Yan et al. [20] found that the addition of Li made the O-H bond of $Ca(OH)_2$ broken more easily, thereby improving the dehydration reaction rate and heat storage efficiency of $Ca(OH)_2$. It indicates that the addition of LiOH mainly changes the dehydration reaction kinetics of $Ca(OH)_2$ and improves its dehydration efficiency.

3. Computational method and model

Computational methods and models in chemistry offer powerful tools for understanding chemical phenomena, predicting molecular behavior, and designing new materials. One important use of computational chemistry is the prediction of molecule structures and characteristics. Chemists can use quantum mechanical approaches such as density functional theory (DFT) and ab initio calculations to correctly describe the electronic structure of molecules and predict features including molecular geometries, energies, and spectroscopic properties.

3.1 Density functional theory (DFT)

Density functional theory (DFT) is a quantum-mechanical atomistic simulation method to compute a wide variety of properties of almost any kind of atomic system: molecules, crystals, surfaces, and even electronic devices when combined with non-equilibrium Green's functions (NEGF).DFT belongs to the family of first principles (ab initio) methods, so named because they can predict material properties for unknown systems without any experimental input. Among these, DFT has earned popularity due to the relatively low computational effort required. The DFT approach is widely applied in organic and inorganic chemistry, materials sciences like metallurgy or ceramics, and for electronic materials, to just name a few areas. These approaches are critical for understanding chemical bonding, reaction processes, and molecular stability. Computational chemistry is used not just to predict molecular properties but also to model chemical reactions. Molecular dynamics (MD) simulations, for example, trace the movement of atoms and molecules over time, revealing information about the dynamics of chemical events, phase transitions, and biomolecular interactions.[23]

3.1.1 Formal Development of Density Functional Theory

In 1964, the perception of DFT was permanently altered. Hohenberg and Kohn [17] proved that DFT accurately describes the electronic behavior of matter. This was achieved by establishing the following remarkable theorem. [18]

Hohenberg-Kohn Theorem I: This theorem states that the ground state properties of a many-electron system are uniquely determined by its electron density F[ρ(r)]. This implies that all the information about the system, including its wavefunction, is embedded in the electron density.

Hohenberg-Kohn Theorem II: This theorem establishes that there exists a universal functional F[*ρ(r)* of the electron density, which, when minimized, yields the ground state energy of the system. The functional F[ρ(r) includes both the kinetic energy of the electrons and the electron-electron interaction energy. The practical implementation of DFT was significantly advanced by Kohn and Sham in 1965, who introduced the concept of Kohn-Sham (KS) equations. These equations map the complex interacting electron problem to a simpler system of non-interacting electrons that have the same electron density as the interacting system.

Kohn-Sham Equations

The Kohn-Sham approach involves solving a set of self-consistent equations for non-interacting electrons in an effective potential. The KS equations are:

$(-2m/\hbar 2\ \nabla^2+V_{eff}(r))\ \psi i\ (r) = \epsilon i\ \psi i\ (r)$

where ψi(r)ψi (r) are the Kohn-Sham orbitals, ϵiϵi are the corresponding orbital energies, and V_{eff} (r)V_{eff} (r) is the effective potential given by:

$V_{eff}(r)=V_{ext}(r) + \int |r-r'|/\rho(r')\,dr' + V_{xc}[\rho(r)]$

Here, V_{ext}(r) is the external potential (e.g., due to nuclei), the second term is the classical electrostatic (Hartree) potential, and V_{xc}[ρ(r) is the exchange-correlation potential, which accounts for the complex many-body interactions.[19]

Exchange-Correlation Functionals

The exchange-correlation potential V_{xc}[ρ(r)] is a crucial component of DFT. It encompasses the effects of electron exchange and correlation, which are not captured by the simple Hartree term. The exact form of V_{xc} is unknown, and various approximations are used in practice:

Local Density Approximation (LDA): Assumes that V_{xc} depends only on the local electron density ρ(r). It is accurate for systems with slowly varying electron densities.

Generalized Gradient Approximation (GGA): Extends LDA by including the gradient of the electron density ∇ρ(r), improving accuracy for systems with rapidly varying densities.

Hybrid Functionals: Incorporate a portion of exact exchange energy from Hartree-Fock theory with the exchange-correlation energy from GGA or LDA, providing improved accuracy for a wide range of systems.

3.4 Ca (OH)2 and CaO cluster preparation Method

The $Ca(OH)_2$/CaO cluster geometries were first created using classical molecular dynamics simulations, which were included into the ABCluster software. ABCluster searches the global as well as the local minima of atomic and molecular clusters. ABCluster uses global optimization to detect local and global minima energy structure on potential energy surfaces (PESs) of molecular clusters. [10] In ABCluster, the energy of the cluster is calculated by considering electrostatics and Lenard-Jones potentials:

$$U_{\mathrm{LJ}} = \sum_{i=1}^{N} \sum_{i<j}^{N} 4\epsilon_{ij} \left(\left(\frac{\sigma_{ij}}{r_{ij}} \right)^{12} - \left(\frac{\sigma_{ij}}{r_{ij}} \right)^{6} \right) \quad (2)$$

Where I and J are the indices of the molecules, iI and jJ are the indices of the atoms in molecules I and J, respectively. riI jJ is the distance between atom iI and jJ . In the ABCluster algorithm, three parameters are needed: the size of the population of trial solutions SN, the scout limit glimit and the maximum cycle number gmax. For more details on the ABCluster code, the reader is redirected to the original work of Zhang and Dolg. [10] For each cluster size of $Ca(OH)_2$ and CaO we have generated more than 30 geometries using ABCluster software. We chose 10–20 of these 30 geometries for full optimization. We only considered geometries that differed from one another. It should be observed that ABCluster generates various geometries that are almost identical. [11] Identical geometries result in the same final structure after full optimization. For cluster optimization, we used VASP (Vienna Ab initio Simulation Package).

Based on density functional theory, Vienna Ab-Initio Simulation Package (VASP) is one of most popular commercial software and plays a very important role in the field of materials simulations. [12], [13] VASP has been widely used to design new materials, reveal microscopic physical phenomena and explore chemical mechanisms, which allows a systematic study for the chemical reactions. [14] However, VASP team only provides the source codes for Linux system, and the software presents flexible input files and standardized output files.[15]

In this work to provide a more stable cluster, $Ca(OH)_2$ and CaO were optimized twice, referred to as Refinements 1 and 2. Following that, we used the final optimization of refinement 2 for property assessment. After optimizing the cluster, we use the vasp output, ozicar, to get the optimum energy of low-lying isomers. To visualize the optimized structure using Vesta, we used

the VASP, CONTCAR file. The binding energy determines the stability of the $(Ca(OH)_2)_n$ and $(CaO)_n$ cluster structures. [16] First, we calculated the binding energies and formation energies of each $Ca(OH)_2$ and CaO cluster both in their pure form and following doping with Li, Li_2, $LiNO_3$, and LiOH.

4. Result and discussion

We investigated the lowest energy structures of $(CaOH)_2$ and CaO clusters using VASP-optimized eV energies. Figure 1-6 depicts the least energy structures of prepared clusters and their isomers for n = 1−10. We also studied binding energy, formation energy and relative stability of each cluster. We report the average bond length and bond angle for the ground state structure and isomers for clusters with N ≤ 10. The details are discussed in this section.

4.1a. Geometries of $Li(CaOH)_{n-1}O_n$ and $LiCa_{n-1}O_n$(n=2−10) clusters

From the four distinct isomers of 1Li-subs- $(CaOH)_2$ with n=2, we chose the most stable one, which had an energy of -38.796 eV. The other three isomers had energies of -38.673 eV, -38.340 eV, and -38.362 eV. Furthermore, isomers with average bond lengths of Ca-O 2.26 Å and Ca-Li 1.90 Å were discovered, together with a bond angle (O-Li-O) = 92.66 °. Additionally, we chose two isomers for 1Li-subs-CaO, whose energies were -10.505 eV and -10.502 eV, the first of which was the most stable. The isomers had an average bond distance of 1.79 Å for Li-O and 2.02 Å for Ca-O, with a bond angle of Li-O-Ca of 96.65 °.

For the 1Li-subs- $(CaOH)_2$ n=3, we also selected four deferent isomers with optimized energies of -60.325 eV, -59.941 eV, -60.279 eV, and -60.1551 eV furthermore, the isomers' average bond angles are Li-O-Ca = 93.33° and Ca-O-Ca = 100.33°, and their average bond distances are Li-O = 1.877 Å and Ca-O = 2.247 Å, of these, isomer 1 with an energy of -60.325 eV was the most stable. Meanwhile, for the CaO, we had three deferent isomers with vasp energies of -17.801 eV, -17.802 eV, and -17.801 eV, and bond distance Li-O = 1.797 Å, Ca-O = 2.247 Å, also with bond angle Li-O-Ca = 95.10°, of these, we discovered that the isomer with -17.802 eV was the most stable.

In reference to 1Li-subs- $(CaOH)_2$, for n = 4, the following isomers were selected: -81.802 eV, -81.589 eV, -81.819 eV, and -81.591 eV. Their average bond distance was Ca-O = 2.417 Å, Li-O = 1.926 Å, and their bond angle was Li-O-Ca = 90.48°. Based on low-lying energy, the isomer with -81.802 eV was found to be the most stable among the others. Comparably, the first of the two isomers of CaO, which have energies of -26.019 eV and -26.004 eV, was the most stable.

At n=5, we find 4 and 3 different isomers when we substitute 1 Li for $(CaOH)_2$ and CaO, respectively. The stable isomer of $(CaOH)_2$ has an energy of -103.621 eV, whereas the other isomers have energies of -103.502, -103.577, and -103.411 eV. They present with average bond angles of Ca-O-Ca = 99.65° and Li1-O3-Ca3) = 86.35°, with average bond distances of Li-O = 1.962 Å, Li-Ca = 2.979 Å, and O-Ca = 2.219 Å. Additionally, for the CaO, the three isomers were present with an average bond distance of Li-O = 1.768 Å, Li-Ca = 3.035 Å, and a bond angle of Li-O-Ca = 94.74°, Ca-O-O = 48.33°. The stable isomer of 3 was present with an energy of -33.609 eV, while the other two had values of -33.508 eV and -33.497 eV.

Six distinct isomers of $(CaOH)_2$ were obtained when 1 Li was substituted for $(CaOH)_2$ and CaO at n = 6. These isomers had average bond distances of Li-O = 1.945 Å, Ca-O = 2.285 Å, Li-Ca = 2.863 Å, and bond angles of Li-O-Ca = 74.37°. The stable isomer was found to have an optimal vasp energy of -125.685 eV, while the remaining five isomers had energies of -125.390 eV, -125.547 eV, -125.547 eV, -125.198 eV, and -125.209 eV. The same was discovered for CaO, where three stable isomers were identified: -40.707 eV, -41.852 eV, and -38.411 eV; the bond angles were Li-O-Ca = 84.21°, the bond distances were Li-O = 1.952 Å and Li-Ca = 2.898 Å. An energy of -41.856 eV was determined for the stable isomer.

Four distinct isomers result from substituting 1 Li for $(CaOH)_2$ and CaO at n=7. Isomers with energies around -147.404 eV show stronger stability for $(CaOH)_2$ substituted Li, whereas the isomer for CaO with -48.860 eV shows the most stability among the other isomers.

When Li is substituted with $(CaOH)_2$ at n=8, the resulting isomers having bond distances of Li-O = 1.929 Å, Ca-O = 2.269 Å, Li-Ca = 2.943 Å, and bond angles Ca-O-Li = 88.62°. They also have energies of -169.260 eV, -169.493 eV, -169.498 eV, -169.369 eV, and the isomer with energy of -169.498 eV exhibit strong stability. Similar results were obtained for CaO, which produced isomers with the following bond distances: Li-O = 1.887 Å, Ca-O = 2.203 Å, Li-Ca = 2.637 Å, and bond angle Li-O-Ca = 79.89°. These isomers had energies of -48.483 eV, -48.860 eV, and -47.795 eV, with the most stable being the one with (-48.860 eV).

We produce four distinct isomers for both $(CaOH)_2$ and CaO in the instance of n=9. The most stable isomer for Li-subs- $(CaOH)_2$ was identified with an energy of -191.595 eV, followed by -191.417 eV, -191.237 eV, and -191.099 eV. The average bond distances were Li-O = 1.870 Å, Ca-Li = 2.945 Å, and Ca-O = 2.364 Å, while the bond angle was Ca-O-Li = 106.50°. Additionally, for CaO, four isomers were found with energies of -64.755 eV, -64.754 eV, -64.764 eV, and -64.766 eV. The isomer with the value of -64.766 eV was stable relative to the

other isomers, and the bond distances were Li-O = 1.787 Å, Ca-O = 2.429 Å, and Li-O-Ca = 83.52°.

In case of n=10 we generate four deferent isomers of 1Li-subs- $(CaOH)_2$ with energies of -214.134 eV, -213.744 eV, -213.383 eV and -213.507 eV, with bond distance of O-Li = 1.865 Å, Ca-O = 2.232 Å, Ca-Li = 3.071 Å, and bond angle of Li-O-Ca = 89.25° and based on low-lying energy the one with energy of -214.134 eV were the most stable and also for CaO we have 4 deferent isomers with optimal energies of -70.396 eV, -72.244 eV, -77.191 eV and -77.030 eV, with bond distance Li-O = 1.780 Å, Ca-Li = 3.055 Å, and bond angle Li-Ca-O = 91.54°, the isomer with energy of -77.191 eV show strong stability relative to others. Figures 1a and 1b illustrate the most stable isomers of $Li(CaOH)_{n-1}O_n$ and $LiCa_{n-1}O_n$ (n=2−10) clusters, respectively.

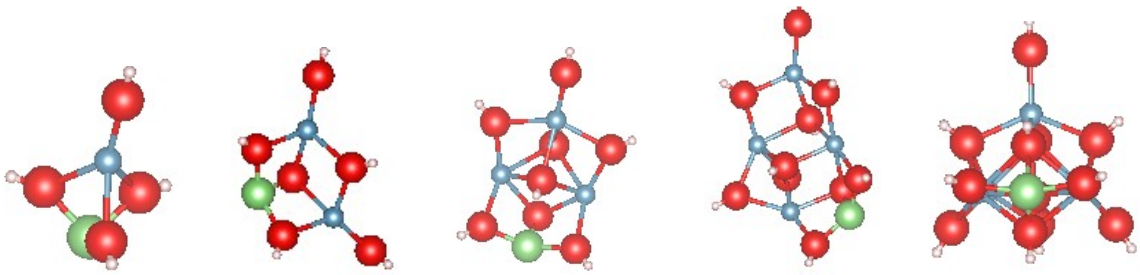

n=2 **n=3** **n=4** **n=5** **n=6**

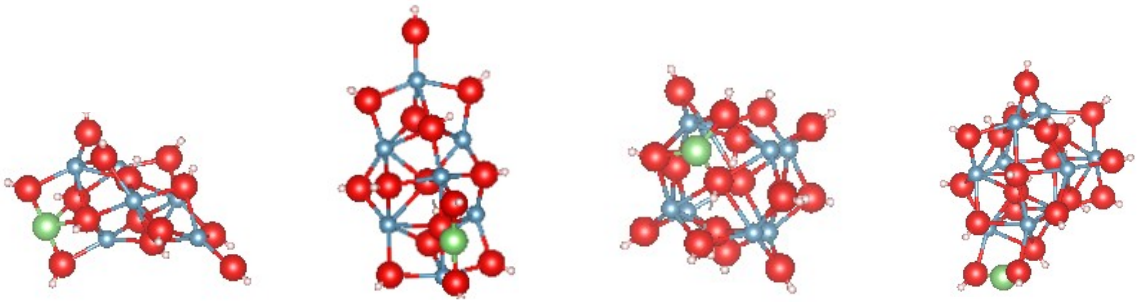

n=7 **n=8** **n=9** **n=10**

FIG. 1a. The most stable Isomer geometries for $Li(CaOH)_{n-1}O_n$ clusters. n= 2-10 [red= O, green = Li, blue black = Ca, and white, grey = H atom]

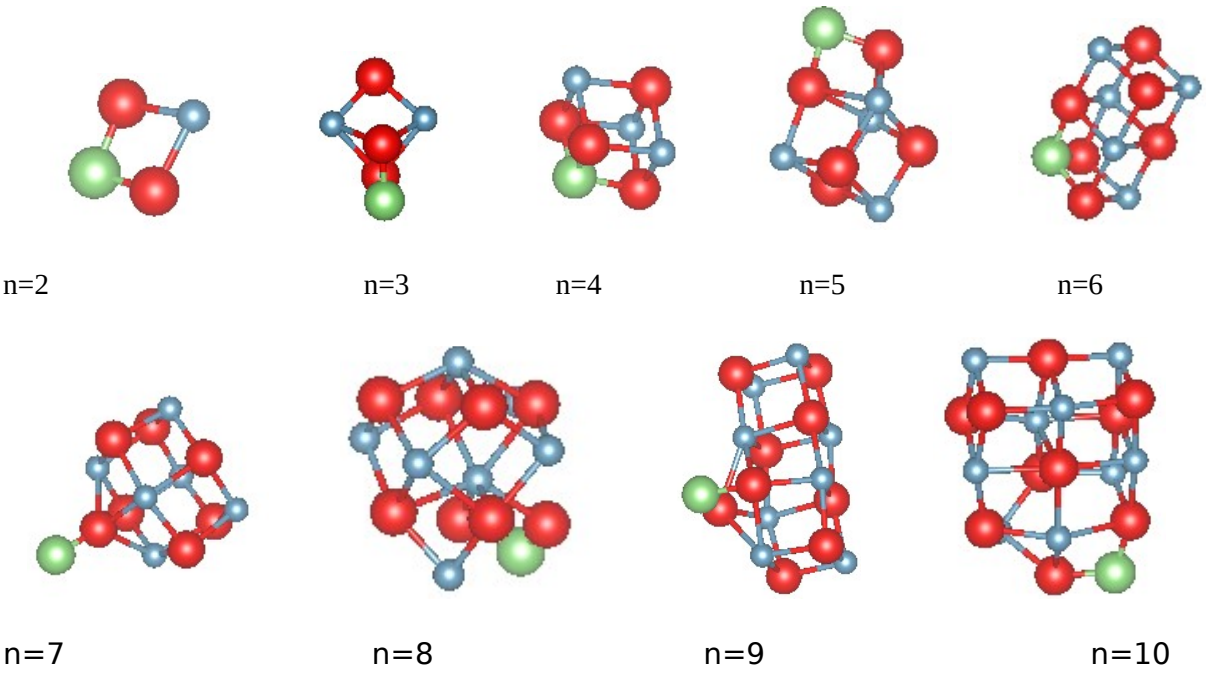

FIG. 1b. The most stable Isomer geometries for $Li(Ca_{n-1}O_n)$ clusters. n= 2-10 [red= O, green = Li, blue black = Ca, and white, grey = H atom]

4.1b. Geometries of $Li_2(CaOH)_{n-1}O_n$ (n=2−10) and $Li_2Can\text{-}1O_n$ (n=2−10) clusters

Substituting 2Li into $(CaOH)_2$ at n=2 results in four distinct isomers with energies of -44.541 eV, -44.172 eV, -44.068, and -43.989 eV. The average bond distance for both Lithium Li-O = 1.790Å, Ca-Li = 2.834 Å, and Ca-O = 2.245 Å, and bond angle Li-O-Ca = 88.45° were observed. The isomer with -44.541 eV was the most stable. Substituting 2Li for $(CaOH)_2$ at n=2 results in increased energy, decreased bond distance, and bond angle, compared to substitution of 1Li indicating $(CaOH)_2$'s strong stability in 2Li-substitution. Similarly, CaO has only one isomer with energy of -14.037 eV, bond distance Li-O = 1.859 Å, Ca-Li = 2.588 Å, and bond angle Ca-O-Li = 82.54°.

At n=3, there are five distinct isomers of 2Li-subs- $(CaOH)_2$ with energies of -66.092 eV, -65.951 eV, -65.916 eV, -65.7937 eV, and -65.542 eV. The average bond distances are Li-O = 1.908 Å, Ca-O = 2.210 Å, Li-Ca = 2.944 Å, and bond angle Ca-O-Li = 90.88°. The isomer with -66.092 eV was stable among the others. CaO has two isomers with different energies (-21.854

eV and -21.860 eV), bond distances (Li-O = 1.845 Å, Ca-O = 2.133 Å, Ca-Li = 2.701 Å), and bond angles (Li-O-Ca = 85.23°). The isomer with -21.860 eV was found to be the most stable.

When we substitute 2Li to $(CaOH)_2$ and CaO at n=4 we have 4 and 2 isomers respectively, the 2Li-subs- $(CaOH)_2$, isomers found with energy of -87.810 eV, -87.598 eV, -87.585 eV, -87.226 eV, with average bond distance Li-O = 1.856 Å, Li-Ca = 3.050 Å, Ca-O = 2.229 Å, and with bond angle Ca-O-Li = 89.25° and the isomer with energy of -87.810 eV was most stable based on low-lying energy. Two isomers of 2Li-subs-CaO were discovered with energies of -29.689 eV and -29.693 eV, bond lengths of Li-O = 1.862 Å, Ca-O = 2.252 Å, Li-Ca = 2.554 Å, and bond angle O-Li-Ca = 56.01°. The isomer with the lowest energy was the most stable.

For n=5 of 2Li-subs- $(CaOH)_2$, we have isomers -109.411 eV, -109.587 eV, -108.983 eV, -109.303 eV and -109.218 eV, with bond distance Li-O = 2.040 Å, Ca-Li = 2.896 Å, Ca-O = 2.186 Å, and bond angle Li-O-Ca = 89.71°. The isomer with -109.587 eV is the most stable. The most stable isomer of 2Li-subs-CaO was -38.110 eV, with bond distances of 1.827 Å, O-Ca = 2.156 Å, Ca-Li = 2.790 Å, and bond angle Ca-O-Li = 82.27°.

We produce five distinct isomers of 2Li-subs- $(CaOH)_2$ for n = 6, ranging in energy from -131.246 eV to -131.197 eV, -131.276 eV, and -131.109 eV. The average bond distances are Li-O = 1.844 Å, Ca-O = 2.216 Å, and Ca-Li = 3.012 Å, with a bond angle of 95.28°. Of these, the isomer with energy of -131.276 eV was the most stable among the others, as determined by low-lying energy. Furthermore, for 2Li-subs-CaO, we have four isomers with optimal energies of -43.080 eV, -45.532 eV, -43.541 eV, and -43.998 eV. The most stable isomer has the following bond lengths: Li-O = 1.926 Å, Ca-O = 2.198 Å, Li-Ca = 2.671 Å, and bond angle: Li-O-Ca = 80.40°.

In general, we observe that the difference between 1Li substitution and 2Li substitution into both $(CaOH)_2$ and CaO in that of the energy of all isomers n = (1-10) is greater in 2Li substitution than in 1Li. Additionally, we observed that the bond length and bond angle of the isomers increased in 2Li substitution than in 1Li substitution. These may lead to longer distance between atoms allowing for dynamic rearrangement maintaining stability. The same procedure was followed for the remaining isomers of n = 7–10. Figures 2a and 2b depict the most stable isomers from two separate clusters: $Li_2(CaOH)_{n-1}O_n$ (n=2−10) and $Li_2Ca_{n-1}O_n$ (where n spans from 2 to 10), respectively.

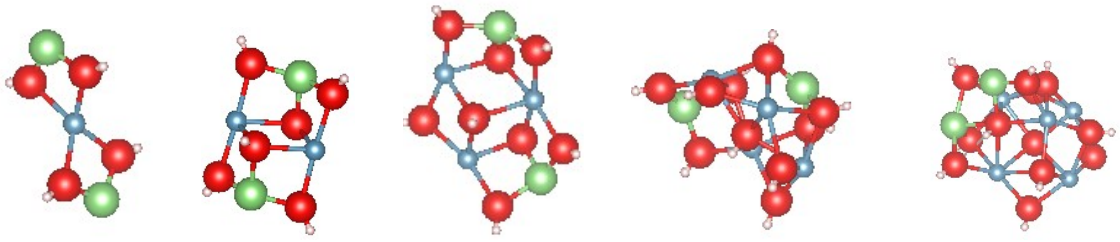

n=2 n=3 n=4 n=5 n=6

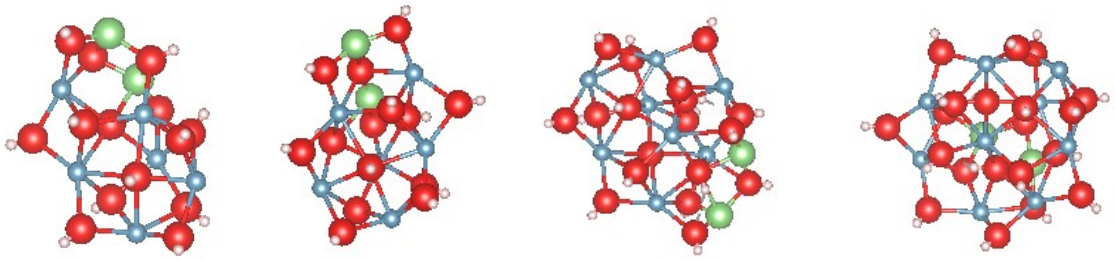

n=7 n=8 n=9 n=10

FIG. 2a. The most stable Isomer geometries for $Li_2(CaOH)_{n-1}O_n$ clusters. n= 2-10 [red= O, green = Li, blue black = Ca, and white, grey = H atom]

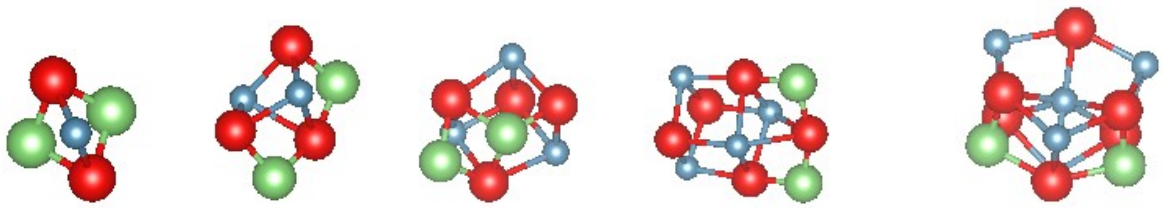

n=2 n=3 n=4 n=5 n-6

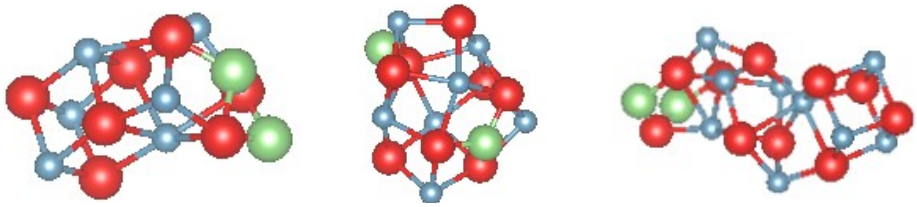

n=7 n=9 n=10

FIG. 2b. The most stable Isomer geometries for $Li_2(Ca_{n-1}O_n)$ clusters. n= 2-10 [red= O, green = Li, blue black = Ca, and white, grey = H atom]

4.1c. Li-i- $(CaOH)_n$ and Li-i-$(CaO)_n$ (n=2−10) clusters

At n = 1, two distinct isomers were generated. In the first isomer, designated as Li interstitial $(CaOH)_2$, the bond lengths were measured as Li-O = 1.813 Å, Ca-O = 2.160 Å, and Li-Ca = 2.819 Å, with a bond angle of Li-O-Ca = 89.95°. Computational simulations using VASP yielded energies of -20.780 eV and -19.866 eV for the two isomers, respectively. The isomer with an energy of -20.780 eV was identified as the most stable configuration.

For the second isomer, denoted as Li interstitial CaO, only one configuration was obtained with an energy of -5.5511 eV. In this isomer, the bond lengths were found to be Ca-O = 1.939 Å and Li-O = 1.657 Å

When examining the introduction of n = 2 Li interstitials into $(CaOH)_2$, three distinct isomers emerge, each characterized by different energies and bond lengths. Specifically, these isomers possess energies of -42.061 eV, -42.033 eV, and -42.048 eV, with corresponding bond lengths measured as Li-O = 1.823 Å, Ca-O = 2.190 Å, and Li-Ca = 3.258 Å. Additionally, they exhibit a bond angle of Li-O-Ca = 108.24°. Among these isomers, the configuration with an energy of -42.061 eV stands out as the most stable.

In the scenario involving Li interstitials in CaO, two isomers are formed, distinguished by energies of -12.9521 eV and -12.444 eV, respectively. The bond distances in these isomers are Li-O = 1.885 Å, Ca-O = 2.123 Å, and Li-Ca = 2.608 Å, while the bond angle is Li-O-Ca = 80.90°. Notably, the isomer with an energy of -12.9521 eV is identified as the most stable configuration.

From the Li interstitials in $(CaOH)_2$ at n = 3, we derived four unique isomers, each characterized by energies of -63.844 eV, -63.799 eV, and -63.233 eV, along with bond lengths of Li-O = 1.827 Å, Ca-O = 2.221 Å, and Ca-Li = 3.316 Å. These isomers also exhibit a bond angle of Li-O-Ca = 109.63°. Among these configurations, the most stable isomer was identified with an energy of -63.844 eV.

Similarly, for the Li interstitials in CaO, three distinct isomers were obtained, featuring bond lengths of Li-O = 1.846 Å, Ca-O = 2.114 Å, and Li-Ca = 2.740 Å, as well as bond angles of Li-O-Ca = 87.28°. The isomer with the lowest energy, -20.212 eV, was determined to be the most stable according to our findings.

Introducing lithium (Li) into calcium hydroxide $(CaOH)_2$ clusters at n = 4 yields four unique isomers, each characterized by energies of -85.242 eV, -85.299 eV, and -85.295 eV, respectively.

These isomers exhibit average bond distances of Li-O = 1.897 Å, Ca-O = 2.350 Å, and Li-Ca = 3.073 Å, alongside a bond angle of Li-O-Ca = 92.07°. The most stable configuration among these isomers was determined to have an energy level of -85.299 eV.

In the case of calcium oxide (CaO), three isomers are observed, with energy levels of -28.997 eV, -26.420 eV, and 27.945 eV, respectively. These isomers feature bond distances of Li-O = 1.717 Å, Ca-O = 2.262 Å, and Li-Ca = 3.546 Å, and a bond angle of Li-O-Ca = 125.45°. The isomer with an energy level of -28.997 eV emerged as the most stable among them.

In the $(CaOH)_2$, Li interstitial with n = 5, we produced four distinct isomers with energies of -107.456 eV, -107.339 eV, -107.454 eV, and -107.200 eV. The isomers had bond distances of Li-O = 1.996 Å, Li-O = 1.936 Å, Li-Ca = 3.196 Å, and bond angle Li-O-Ca = 94.78°. The most stable isomer was Li-O = 107.456 eV. Similarly, for CaO, we had two isomers with bond distances of Li-O = 1.811 Å, Ca-O = 2.050 Å, Li-Ca = 2.682 Å, and bond angle Ca-O-Li = 82.13°. Their energies were -36.388 eV and -36.518 eV, with the most stable being the one with -36.518 eV.

For $(CaOH)_2$ with Li interstitials at n = 6, we identified five unique isomers with energies of -129.206 eV, -129.184 eV, -129.250 eV, and -129.063 eV. These isomers exhibit bond distances of Li-O = 1.847 Å, Ca-O = 2.359 Å, and Ca-Li = 2.811 Å, along with a bond angle of Li-O-Ca = 87.11°. Among these isomers, the most stable configuration was determined to have an energy of -129.250 eV.Similarly, for CaO, three isomers were produced with energies of -42.346 eV, -43.910 eV, and -43.901 eV. The most stable isomer among these is characterized by an energy of -43.910 eV.

Comparable procedures were followed for the remaining isomers of $(CaOH)_2$ and CaO with Li interstitials at n = 7–10. Various isomers with different energies, bond distances, and bond angles were generated, and the most stable isomer in each case was identified based on its lower energy level. Figures 3a and 3b illustrate the most stable isomers of Li-i-(CaOH)n and Li-i-(CaO)n clusters, respectively.

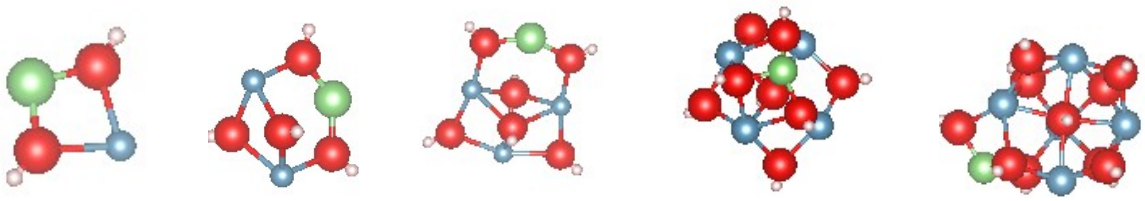

n=1 n=2 n=3 n=4 n=5

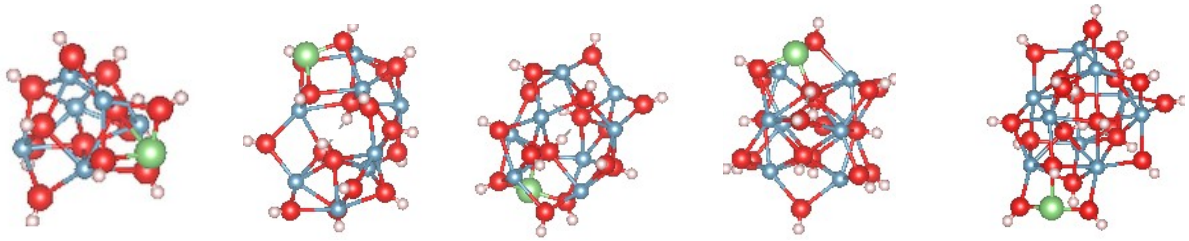

n=6 n=7 n=8 n=9 n=10

FIG. 3a. The most stable Isomer geometries for Li-i-$((CaOH)_2)_n$ clusters. n= 2-10 [red= O, green = Li, blue black = Ca, and white, grey = H atom]

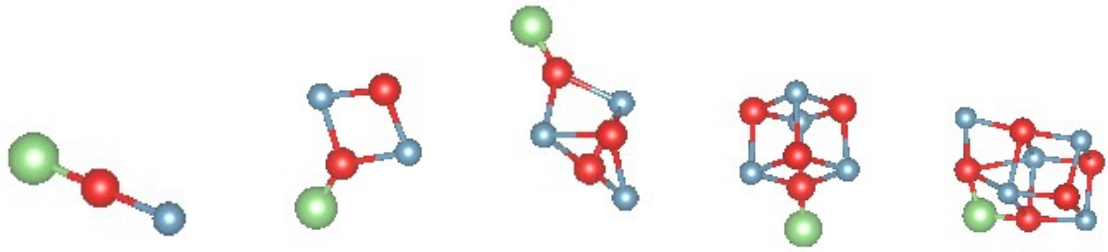

n=1 n=2 n=3 n=4 n=5

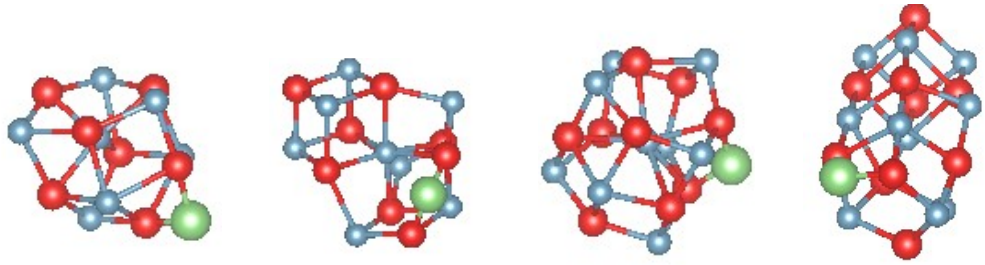

n=6 n=8 n=9 n=10

FIG. 3b. The most stable Isomer geometries for Li-i-$(CaO)_n$ clusters. n= 2-10 [red= O, green = Li, blue black = Ca, and white, grey = H atom]

4.1d. $LiNO_3$ - $(CaOH)_n$ (n=1-10)

When $LiNO_3$ is introduced into $(CaOH)_2$ at n = 1, three distinct isomers are generated, exhibiting energies of -41.857 eV, -41.227 eV, and -41.302 eV, respectively. The most stable isomer among them is characterized by an energy of -41.857 eV. The bond distances in this configuration are

N-Ca = 2.762 Å, N-O = 1.227 Å, Li-O = 1.809 Å, and N-Li = 5.585 Å, while the bond angles are measured as O-N-Ca = 57.94° and Li-O-Ca = 89.18°.

Unfortunately, due to limitations within our system, we were unable to generate an isomer for the CaO cluster with $LiNO_3$.

At n = 2, we generated three distinct isomers of $LiNO_3$-$(CaOH)_2$, characterized by energies of -63.086 eV, -62.984 eV, and -62.873 eV, respectively. The bond lengths observed in these configurations were N-O = 1.309 Å, Ca-O = 2.345 Å, Li-O = 1.801 Å, Ca-Li = 2.832 Å, and Ca-N = 2.761 Å. Additionally, the bond angles were measured as Li-O-Ca = 88.91° and Ca-O-N = 93.83°.

For n = 3, we obtained three distinct $LiNO_3$-$(CaOH)_2$ configurations. In these configurations, the bond lengths were measured as Li-O = 2.060 Å, Ca-O = 2.190 Å, Li-Ca = 2.952 Å, Ca-N = 2.779 Å, and N-O = 1.305 Å. Additionally, the bond angles were determined to be Li-O-Ca = 92.04° and Ca-O-N = 94.32°. The optimization energies associated with these configurations were -84.590 eV, -85.009 eV, -84.587 eV, and -85.971 eV, respectively.

There are three unique isomers for $[Ca(OH)_2]_4$ $LiNO_3$, distinguished by bond angles of Ca-O-N = 130.76° and Ca-O-Li = 109.50°, as well as bond distances of Li-Ca = 3.029 Å, Li-O = 1.931 Å, N-O = 1.294 Å, and Ca-O = 2.326 Å. These isomers possess low energy levels, measured at -106.435 eV, -106.372 eV, -106.573 eV, and -106.378 eV, respectively. The most stable isomer among them is characterized by an energy of -106.394 eV.

The cluster $[Ca(OH)_2)_5]$ $LiNO_3$ possesses four isomers, with bond energies of -128.479 eV, -128.579 eV, -128.564 eV, and -128.573 eV, and corresponding bond distances of N-O = 1.292 Å, N-Ca = 2.894 Å, Ca-O = 2.419 Å, Li-O = 2.288 Å, Li-Ca = 2.901 Å, and bond angles of Li-O-Ca = 90.00° and N-O-Ca = 131.82°. The isomer with an energy of -128.579 eV was determined to be the most stable.

Four unique isomers were identified for the cluster $[Ca(OH)_2]_6$ $LiNO_3$, each characterized by low energy ranging from -150.394 eV to -150.382 eV. These isomers displayed bond distances of N-O = 1.317 Å, N-Ca = 2.893 Å, Ca-O = 2.428 Å, Li-O = 1.887 Å, and Li-Ca = 3.082 Å. Additionally, the bond angles observed were Li-O-Ca = 97.28° and N-O-Ca = 97.49°. The most stable isomer among them was determined to have an energy of -150.394 eV.

At n = 7, we produced four distinct isomers of $LiNO_3$-$(CaOH)_2$, each exhibiting different energy levels and bond distances. The energies of these isomers ranged from -172.450 eV to -171.962

eV. The bond distance N-O remained consistent at 1.292 Å across all isomers. However, the distances between other atoms varied: N-Ca was 3.347 Å, Ca-O was 2.332 Å, Li-O was 1.960 Å, and Li-Ca was 3.367 Å. Additionally, the bond angles differed, with Li-O-Ca at 92.97° and N-O-Ca at 138.53°. The isomer with the lowest energy level (-172.450 eV) was identified as the most stable.

Furthermore, we generated four distinct isomers of $LiNO_3$-$[(CaOH)_2]_8$, each characterized by average bond distances of N-O = 1.231 Å, N-Ca = 2.911 Å, Ca-O = 2.430 Å, Li-O = 2.033 Å, and Li-Ca = 2.867 Å. Additionally, the bond angles observed were Li-O-Ca = 81.76° and N-Ca-O = 26.80°. The lowest energy levels of these isomers were found to be -194.142 eV, -194.429 eV, -194.396 eV, and -194.639 eV, with the most stable among them being -194.639 eV.

Similarly, at n = 9, the $LiNO_3$-$(CaOH)_2$ isomers were generated, yielding optimization energies of -216.194 eV, -215.761 eV, -215.396 eV, and -215.878 eV. The bond distances observed were Li-O = 1.947 Å, Ca-O = 2.241 Å, Li-Ca = 3.042 Å, and Ca-N = 3.400 Å. The bond angles measured were Ca-O-Li = 90.14° and Ca-O-N = 135.42°. The most stable isomer among them was found to have an energy level of -216.194 eV.

Furthermore, the same methodology was applied for n = 10. Please refer to Figure 4 for a comprehensive overview of the most stable isomers of the $LiNO_3$-(CaOH)n cluster, where n ranges from 1 to 10.

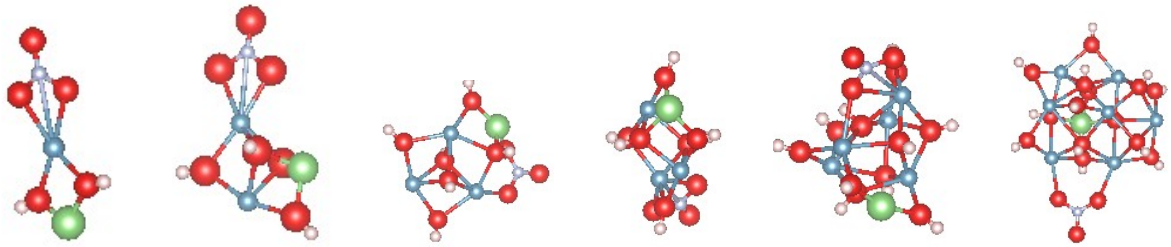

n=1 n=2 n=3 n=4 n=5 n=6

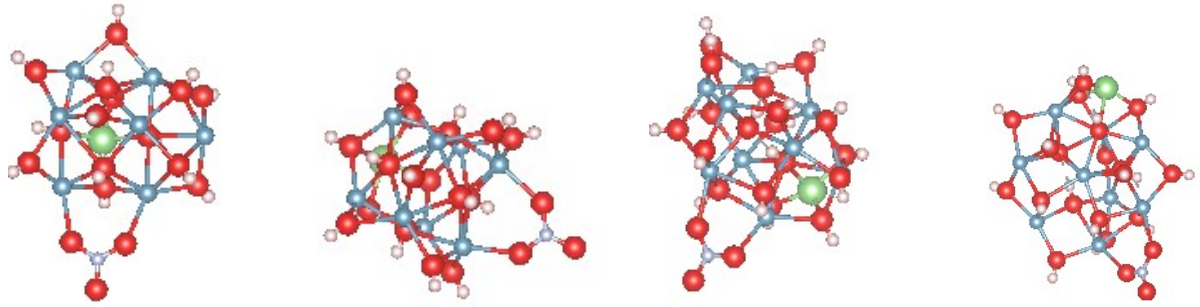

n=7 n=8 n=9 n=10

FIG.4 Most stable isomers of LiOH-Ca(OH)$_n$ clusters (n=1-10) [red= O, green = Li, blue black = Ca, and white, grey = H, white = N atom]

4.1e. LiCl-(Ca(OH)$_2$)$_n$ (n=1-10) clusters

Preparation of Isomers: The preparation involved synthesizing three to four distinct isomers of LiCl-(Ca(OH)$_2$)$_n$ (n=1-10) clusters. Isomers refer to molecules with the same molecular formula but different arrangements of atoms. In this case, by using ABcluster software we have created multiple arrangements of lithium chloride (LiCl) and calcium hydroxide (Ca(OH)$_2$) molecules.

Energy Optimization: Using VASP (Vienna Ab-initio Simulation Package), the energies of these clusters were optimized. The optimized energies ranged from 24.529 eV to -220.479 eV for clusters with n values from 1 to 10. These energy values are crucial as they indicate the stability of the clusters, with more negative values indicating greater stability.

Bond Distances: The average bond distances within these clusters were determined. For example, the average bond distances between different atom pairs such as Cl-Ca = 2.511 Å, Ca-O = 2.190 Å, Li -O = 1.810 Å, Ca-Li = 2.825 Å to Cl-Ca = 2.836 Å, Li-O = 1.979 Å, Ca-Li = 3.047 Å for clusters n=1-10. These distances provide insights into the spatial arrangement of atoms within the clusters and help understand the bonding interactions between them.

Bond Angles: Similarly, the average bond angles within the clusters were Ca-O-O = 50.12°, Cl-Ca-O = 140.13°, Cl-Ca-Ca = 50.14°, Li-O-O = 38.14° for interval clusters of n=1-10, provide information about the geometric arrangement of atoms and the molecular structure of the clusters. They also influence the stability and reactivity of the clusters.

Identification of Most Stable Isomers: Based on the energy values obtained, the most stable isomers were identified. These are the configurations of the clusters that have the lowest energy, indicating greater stability and potentially more favorable properties for practical applications.

The figure below, Figure 5, illustrates the most stable structure of LiCl-$(Ca(OH)_2)_n$.

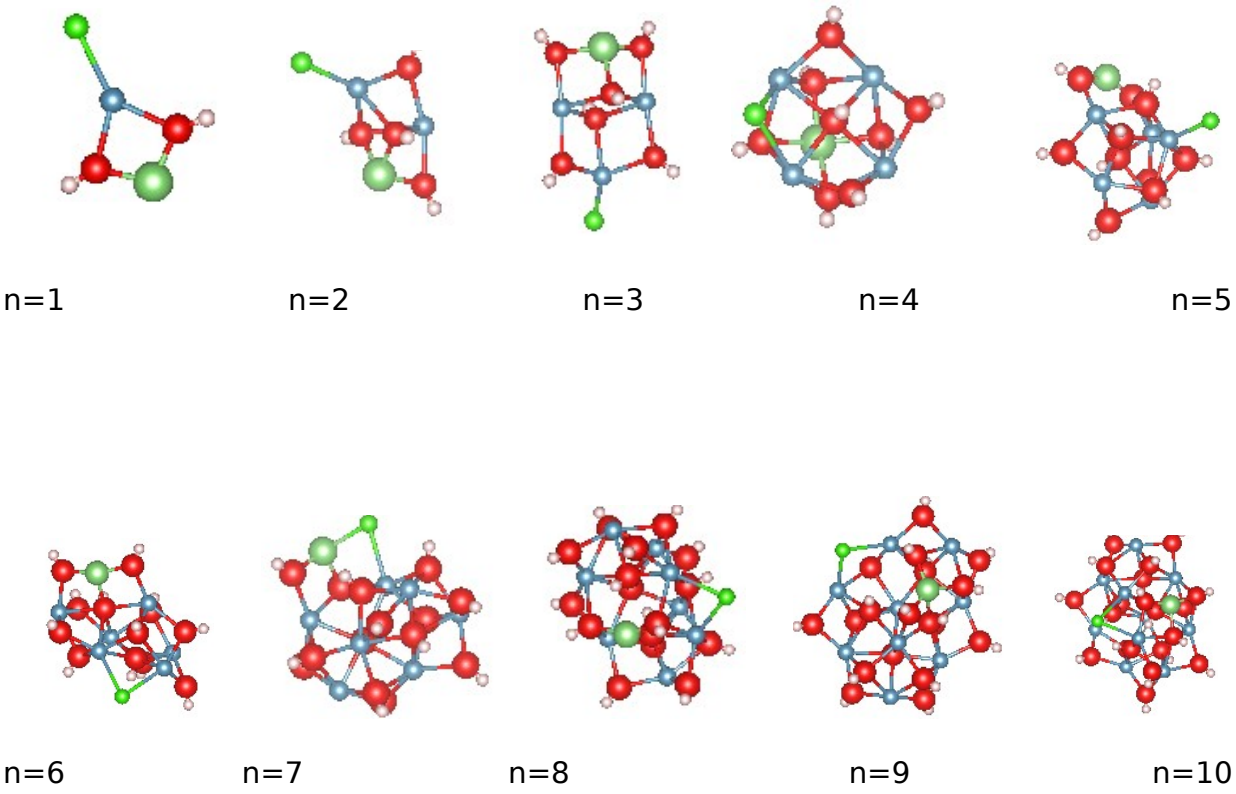

FIG.5 Most stable isomers of LiCl-$(Ca(OH)_2)_n$ (n=1-10) clusters [red= O, green = Li, blue black = Ca, and white, grey = H, shine green = Cl atom]

4.1f. LiOH- $(Ca(OH)_2)_n$ (n=1-10)

We have generated clusters using ABcluster software for LiOH- $(Ca(OH)_2)_n$ by generating each integer value of n from 1 to 10. For each cluster isomer, we obtained approximately three to four distinct arrangements, resulting in a diverse range of structural possibilities. Our meticulous analysis, which included examining bond lengths, bond angles, and optimizing energies using the Vienna Ab-initio Simulation Package (VASP), allowed us to scrutinize the properties of

these isomers. Our investigation enabled us to identify the most stable configurations within each cluster size, ranging from n=1 to n=10. The results of our analysis are presented in the table below, which provides a detailed overview of the identified isomers, including their respective structural characteristics and associated energies. And the most stable isomers of these cluster were shown in figure 6 below.

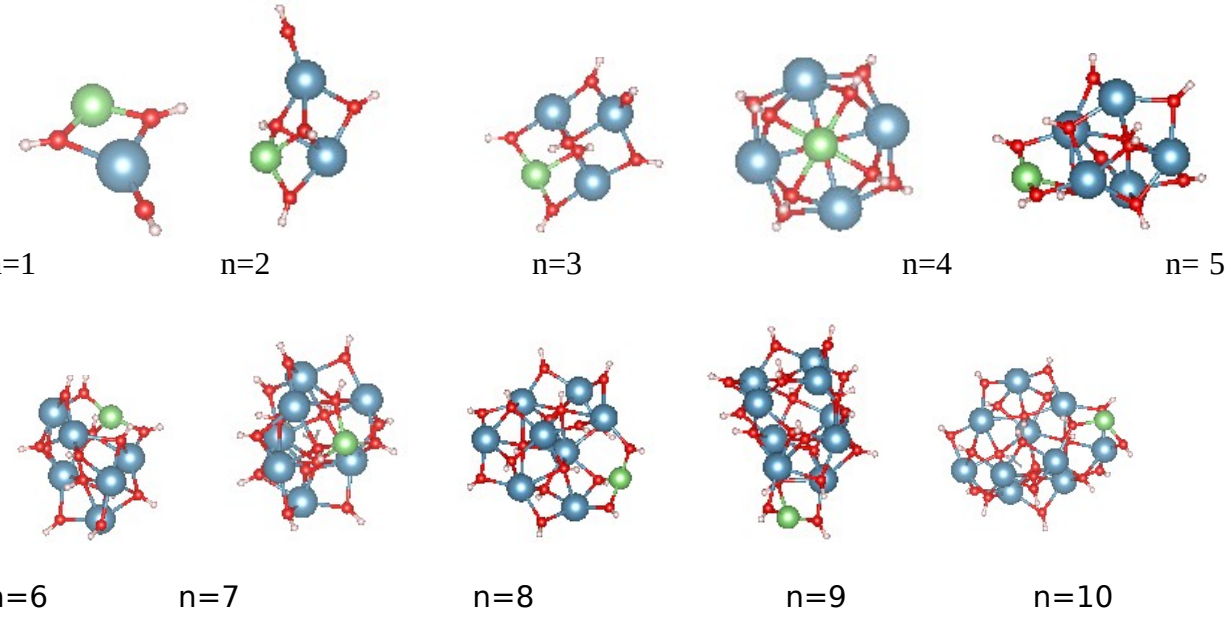

FIG.6 Most stable isomers of LiOH- $(Ca(OH)_2)_n$ (n=1-10) clusters [red= O, green = Li, blue black = Ca, and white, grey = H atom]

4.2 Energetic Properties

4.2.1 Pure (CaOH)2 /CaO clusters

The expression for the formation energy of clusters of Ca((OH)$_2$)n and (CaO)n, in terms of the cluster size n, in their pure state without any doping, can be formulated as:

$$E_{formation} = E_{[Ca(OH)2]n} - nE_{Ca} - nEO_2 - nE_{H2}] \quad (3)$$

$$E_{formation} = E_{[(CaO)n} = nE_{Ca} - nE_{O2}] \quad (4)$$

Where E_{Ca}, energy of calcium metal and E_{O2}, E_{H2},energy of Oxygen and Hydrogen molecules, respectively. The calculation result of average formation energy is plotted in fig. 7 as function of cluster size.

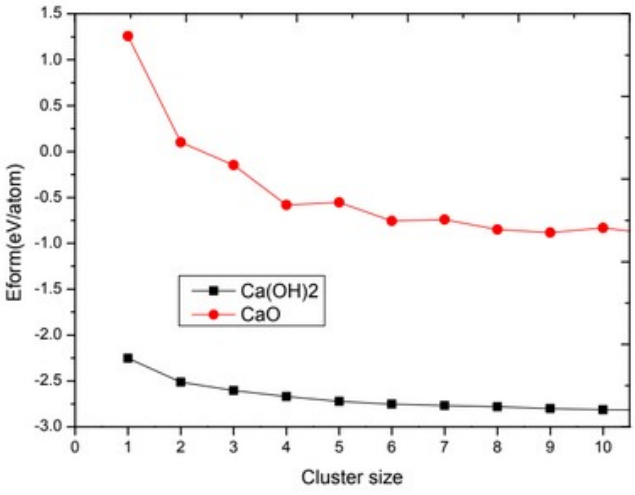

Fig 4. Formation energy (eV) vs cluster size n

The formation energy of a cluster is a measure of the energy change associated with its formation from its constituent atoms or molecules. The formation energies of Ca(OH)2]n and CaO clusters

decreased smoothly as the cluster size increased. indicating enhanced stability as the cluster grows. However, the stability of a cluster is not solely determined by its formation energy.

The binding energy E_b per atom for the individual clusters gives information on the stability of the cluster. [24]

To illustrate the stability of $Ca((OH)_2)_n$ and $(CaO)_n$ clusters, the binding energy per $Ca(OH)_2$/CaO has been calculated as follows

$$B_E\{CaO\} = n^{-1}\,[nE\,Ca + nE\,O - E\,(CaO)_n] \quad (5)$$

$$B_E\{Ca(OH)_2\} = n^{-1}\,[nE\,Ca + nE\,O + nE\,H - E\,[(Ca(OH)_2]n \quad (6)$$

where n represents the size of the clusters and E_{Ca}, E_O, and E_H represent the energies of the isolated Ca, O, and H atoms, respectively. The calculated average binding energy is plotted in fig.8a as a function of the cluster size n,

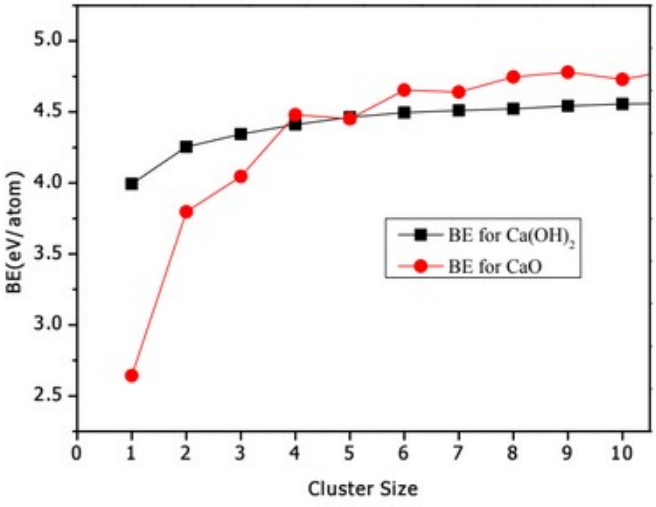

a

FIG. 8 (a) Average binding energies (BE) of cluster size n for $Ca((OH)_2)_n$ and $(CaO)_n$ clusters (n=1−10).

Clearly, the average binding energies of both $Ca(OH)_2$ and CaO increased with increasing cluster size for n = 1-10. The overall behavior of $Ca(OH)_2$ is similar to that observed for the $(CaO)_n$ system. That is, the binding energy increase with respect to the number of cluster sizes.

Table 1 shows the total binding and formation energy data for the Ca(OH)2/CaO cluster n = (1-10).

Table 1. Binding Energy and Formation Energy, of $Ca(OH)_2$ and CaO.

Cluster size	Binding Energy of $Ca(OH)_2$ (eV)	Formation Energy of $Ca(OH)_2$ (eV)	Binding Energy of CaO (eV)	Formation Energy of CaO (eV)
1	3.994	-2.252	2.641	1.256
2	4.254	-2.512	3.797	0.101
3	4.344	-2.602	4.045	-0.147
4	4.410	-2.669	4.480	-0.583
5	4.463	-2.721	4.452	-0.554
6	4.495	-2.753	4.654	-0.756
7	4.509	-2.767	4.640	-0.742
8	4.523	-2.781	4.747	-0.849
9	4.542	-2.800	4.773	-0.882
10	4.555	-2.813	4.725	-0.831

4.2.2 Li Doped $(CaOH)_2$/CaO clusters

I. Binding Energy

To examine the stability of $Ca(OH)_2$/CaO clusters, we conduct substitutional doping by replacing calcium (Ca) atoms with lithium (Li) and lithium dimers (Li_2). This process involves systematically incorporating Li and Li_2 into the cluster structure to assess the resulting changes in stability and properties. The stability of the $LiCa_{n-1}(OH)_2]n$, $Li_2Ca_{n-1}(OH)_2]n$, $LiCa_{n-1}O_n$, and $Li_2Can_{-1}O_n$ cluster structures can be determined by the binding energy. First, we calculated the binding energy of each cluster as follows

$$BE_{LiCan-1[(OH)2]n} = (n\text{-}1E_{Ca} + 2nE_O + 2nE_H + nE_{Li} - E_{LiCan-1[(OH)2]n})/5n \quad (7)$$

$$BE_{Li2Can-1(OH)2]n} = (n\text{-}1E_{Ca} + 2nE_O + 2nE_H + 2nE_{Li} - E_{Li2} - E_{LiCan-1[(OH)2]n})/6n \quad (8)$$

$$BE_{LiCan-1On} = (n\text{-}1E_{Ca} + 2nE_O + E_{Li} - E_{LiCan-1On})/2n \quad (9)$$

$$BE_{LiCan-1On} = (n\text{-}1E_{Ca} + 2nE_O + E_{Li} - E_{LiCan-1On})/3n \quad (10)$$

Where BE signifies the binding energy, E_{Ca}, E_O, E_H, and E_{Li} denote the energy of a single Calcium, Oxygen, Hydrogen, and Lithium atom, and $E_{LiCan-1On}$ denotes the cluster energy.

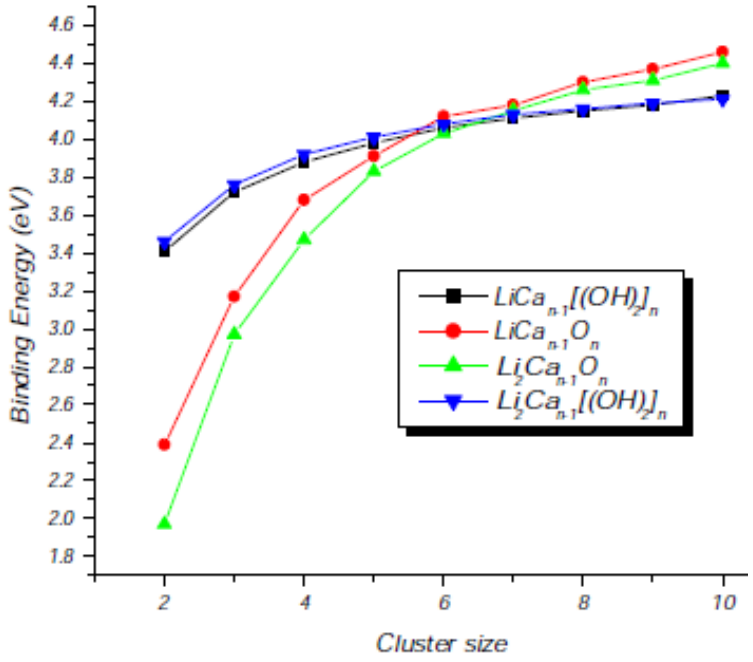

Fig.9a. Size dependence of the binding energies per atom (eV/atom) for the $LiCa_{n-1}(OH)_2)n$, $LiCa_{n-1}O_n$, $Li_2Ca_{n-1}(OH)_2)n$ and $Li_2Ca_{n-1}O_n$ clusters.

The size dependence of the binding energy per atom for clusters with (n = 1-10) is shown in Figure 9a. For $LiCa_{n-1}(OH)_2)n$ clusters, the binding energy increases with cluster size, reaching approximately 4.4 eV at the largest size. Similarly, $LiCa_{n-1}O_n$ clusters exhibit an increasing

binding energy trend, reaching just below 4.4 eV. The Li_2 $Ca_{n-1}O_n$ clusters start with a lower binding energy but also show an upward trend, reaching around 4.2 eV.

Lastly, Li_2 Ca_{n-1} $(OH)_2$)n clusters follow a binding energy trend similar to $LiCa_{n-1}(OH)_2)n$, achieving nearly 4.4 eV at the largest size. The above findings highlight a distinct trend marked by a consistent enhancement in the stability of $Ca(OH)_2$/CaO clusters, achieved through the technique of substitutional doping with lithium (Li) and lithium dimers (Li_2).

The average binding energies of the Li-doped $Ca(OH)_2$ and Li-doped CaO clusters are slightly higher than those of the corresponding pure $Ca(OH)_2$ and CaO clusters. This indicates that doping with a Li atom enhances the stability of both $Ca(OH)_2$ and CaO clusters.

To further investigate the stability of $Ca(OH)_2$/CaO clusters, we introduced interstitial doping by incorporating lithium (Li) and various lithium compounds (LiX), where X represents OH, Cl, and NO_3. We then calculated the binding energy for these doped clusters to understand the effects of these modifications on their stability.

$$BE_{Li\text{-}i\text{-}Ca(OH)2} = nE_{Ca} + 2nE_O + 2nE_H + nE_{Li} - E_{Li\text{-}i\text{-}Ca(OH)2}\ /6n \quad (11)$$

$$BE_{Li\text{-}i\text{-}CaO} = nE_{Ca} + nE_O + nE_{Li} - E_{Li\text{-}CaO}/6n \quad (12)$$

$$BE_{LiCl\text{-}Ca(OH)2} = nE_{Ca} + 2nE_O + 2nE_H + nE_{Cl} - E_{LiCl\text{-}Ca(OH)2}\ /7n \quad (13)$$

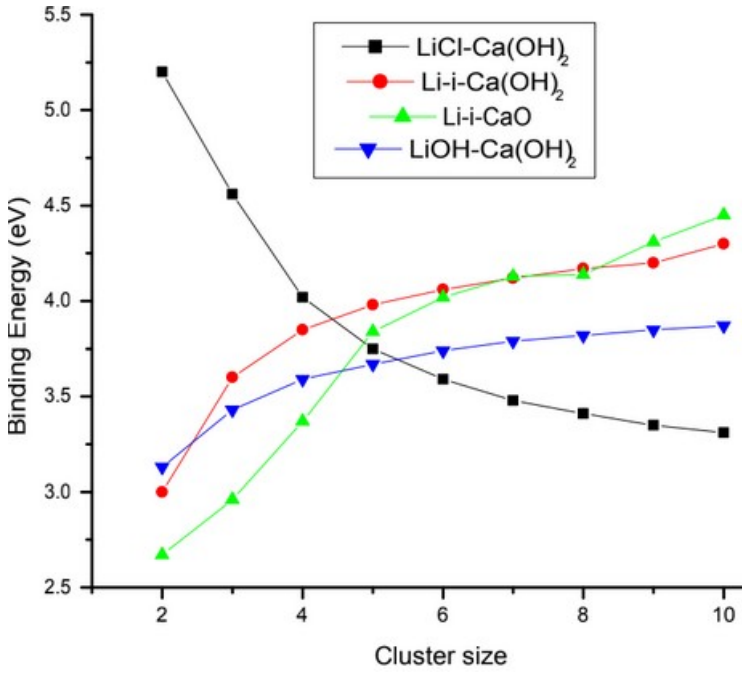

Fig.9b. Size dependence of the binding energies per atom (eV/atom) for the LiCl-$Ca(OH)_2$, Li-i-$Ca(OH)_2$, Li-i-CaO, and LiOH-$Ca(OH)_2$.

The graph shows the binding energy (in eV) versus cluster size for four different types of clusters: LiCl-$Ca(OH)_2$, Li-i-$Ca(OH)_2$, Li-i-CaO, and LiOH-$Ca(OH)_2$. Here is an overview of the trends in the data:

The binding energy of LiCl-$Ca(OH)_2$ falls as cluster size increases from 2 to 10, from roughly 5.0 eV to 3.0 eV. The observed effects are attributed to the electrostatic force of attraction between lithium ions (Li^+) and chlorine ions (Cl^-). This attractive force significantly influences the binding energy to decrease.

On the other hand, Li-i-$Ca(OH)_2$ and Li-i-CaO exhibit increasing binding energy trends with increasing cluster size, rising from 3.3 eV to 3.9 eV and 3.3 eV to 4.0 eV, respectively. LiOH-$Ca(OH)_2$ has a rising binding energy trend, but less steep than Li-i-CaO. These trends indicate that the stability of each cluster type varies with size, with LiCl-$Ca(OH)_2$ becoming less stable and the others becoming more stable.

II. Second Order Energy

The second-order difference in cluster energies (Δ^2E) is a widely used metric for determining the stability of clusters. This method involves assessing the energy differences between clusters of varying sizes to identify particularly stable configurations. We applied this technique by using a specific formula to calculate the second-order energy difference (Δ^2E) for pure calcium hydroxide ($Ca(OH)_2$) and calcium oxide (CaO) clusters. These calculations were performed for both undoped clusters and clusters doped with lithium (Li) and lithium dimers (Li_2). Additionally, for $Ca(OH)_2$ clusters, we extended our calculations to include doping with various lithium compounds (LiX), where X represents different anions: chloride (Cl), nitrate (NO_3), and hydroxide (OH). This comprehensive approach allows us to compare the stability of different doped and undoped cluster configurations systematically.

$$\Delta^2E_{\{Ca(OH)2\}n} = E_{(Ca(OH)2]\,n+1} + E_{(Ca(OH)2]\,n-1} - 2E_{(Ca(OH)2]\,n} \quad (14)$$

$$\Delta^2E_{CaOn} = E_{(CaO)\,n+1} + E_{(CaO)\,n-1} - 2E_{(CaO)n} \quad (15)$$

$$\Delta^2E_{LiCl\text{-}Ca(OH)2} = E_{LiCl\text{-}Ca(OH)2\,n+1} + E_{LiCl\text{-}Ca(OH)2\,n-1} - 2E_{LiCl\text{-}Ca(OH)2\,]n} \quad (16)$$

$$\Delta^2E_{LiOH\text{-}Ca(OH)2} = E_{LiOH\text{-}Ca(OH)2\,n+1} + E_{LiOH\text{-}Ca(OH)2\,n-1} - 2E_{LiOH\text{-}Ca(OH)2]n} \quad (17)$$

Δ^2E represents second-order energy.

The average calculation results for plotting the second order energy as a function of cluster size are shown in Figure 10 below

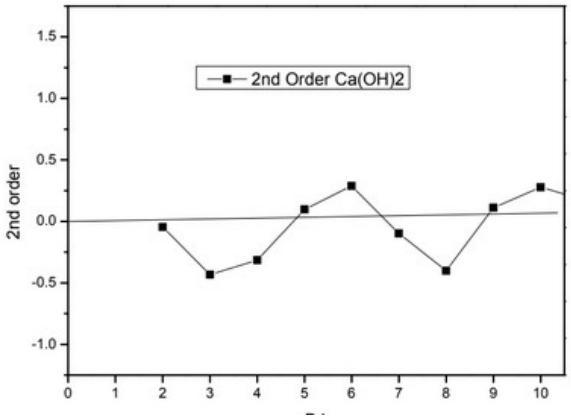
2nd Order Ca(OH)2
2nd order
1.5
1.0
0.5
0.0
-0.5
-1.0
0 1 2 3 4 5 6 7 8 9 10

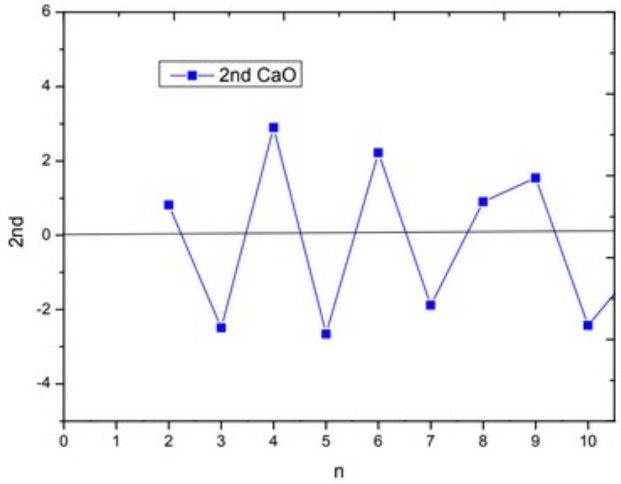
2nd CaO
2nd
6
4
2
0
-2
-4
0 1 2 3 4 5 6 7 8 9 10
n

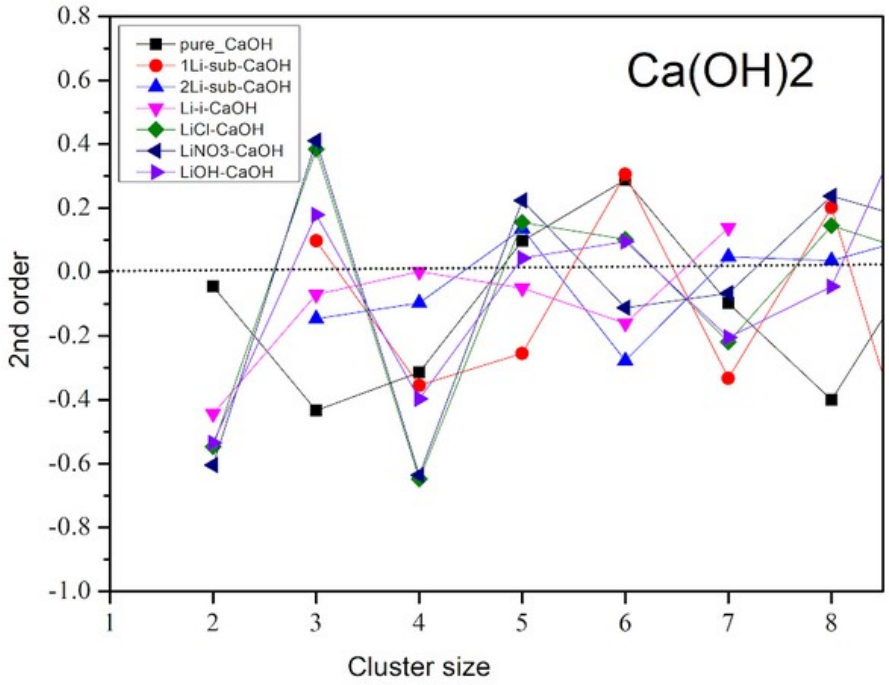

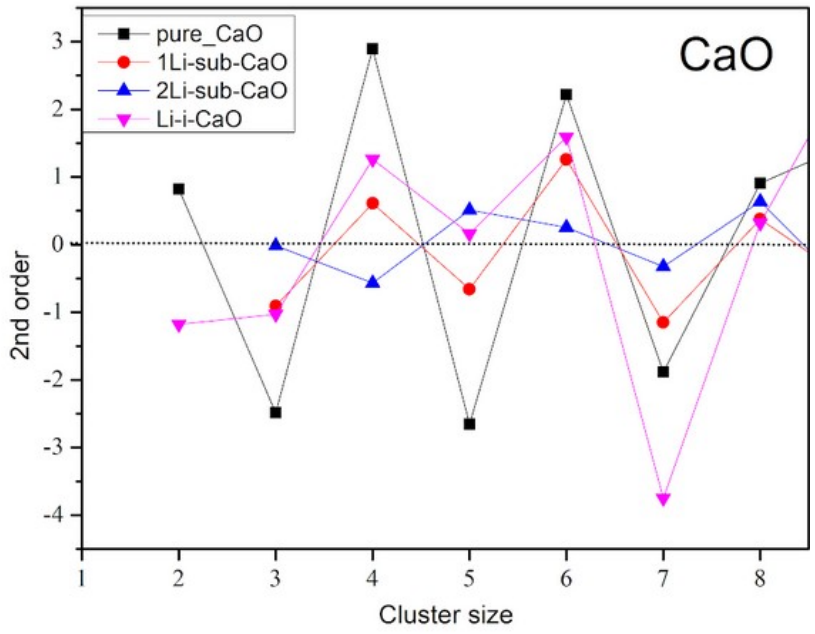

Fig.10 Second Order energy of (CaO)n and $[Ca(OH)_2]n$ n = 1-10 In the Δ^2E figure, upward peaks represent more stable clusters, and downward peaks indicate less stable clusters.

In Fig. 10, the Δ^2E of pure $[Ca(OH)_2]n$ clusters shows alternating peaks: upward at n=6,9,10 and downward at n=2,4,3,7,8, indicating greater stability for n=6,9,10 compared to n=2,4,3,7,8. Similarly, (CaO)n clusters exhibit both upward (n=4,6) and downward peaks, suggesting higher stability for $(CaO)_4$ and $(CaO)_6$ clusters.

Li-sub-$Ca(OH)_2$ exhibits improved stability in cluster sizes 3, 6, and 8 compared to pure $Ca(OH)_2$. However, slight instabilities are observed at sizes 4 and 7. In contrast, 2Li-sub-$Ca(OH)_2$ displays higher stability at sizes 5, 7, and 8, with unstable clusters at sizes 2, 4, and 6, showing significant dips at size 6, indicating instability. Li-i-$(CaOH)_2$ displays higher variability, with unstable clusters at sizes 2 and 6, and stable clusters at sizes 7 and above. LiCl-$Ca(OH)_2$ shows stability at cluster size 3 and a peak at size 6, while sizes 2 and 4 exhibit significant instability. $LiNO_3$-$Ca(OH)_2$ is generally more stable with peaks at sizes 3 and 6, and unstable clusters at sizes 2 and 4, displaying smoother variations compared to LiCl and Li-i modifications.

Table 2 shows the overall calculation results of second order energy for both $Ca(OH)_2$ and CaO clusters at the pure and doped levels.

Cluster Type	**n**	**Pure**	**1Li-sub**	**2Li-sub**	**Li-i**	**LiCl**	**$LiNO_3$**	**LiOH**
CaO Clusters	1							
	2	0.818			-1.18			
	3	-2.487	-0.91	-0.01	-1.03			
	4	2.896	0.61	-0.57	1.26			
	5	-2.651	-0.66	0.51	0.16			
	6	2.218	1.26	0.26	1.59			
	7	-1.883	-1.15	-0.32	-3.75			
	8	0.906	0.38	0.64	0.32			

	9	1.540	-0.61	-0.80	2.87			
	10							
$Ca(OH)_2$Clusters	**n**	**Pure**	**1Li-sub**	**2Li-sub**	**Li-i**	**LiCl**	**$LiNO_3$**	**LiOH**
	1							
	2	-0.045			-0.44	-0.55	-0.60	-0.54
	3	-0.433	0.10	-0.15	-0.07	0.38	0.41	0.18
	4	-0.314	-0.36	-0.10	0.00	-0.65	-0.64	-0.40
	5	0.097	-0.26	0.14	-0.05	0.15	0.22	0.04
	6	0.288	0.31	-0.28	-0.16	0.10	-0.11	0.09
	7	-0.098	-0.33	0.05	0.14	-0.22	-0.07	-0.21
	8	-0.400	0.20	0.04	3.52	0.15	0.24	-0.05
	9	0.111	-0.85	0.12	-4.16	0.04	0.15	0.67
	10							

Table 2: Second Order Energies of $Ca(OH)_2$ and CaO Clusters (n = 1-10)

After analyzing the energy calculations and relative stability of the clusters, we identified the most stable clusters among $Ca(OH)_2$ and CaO for n= 1-10. Interestingly, the cluster with n=6 was found to be the most stable for both $Ca(OH)_2$ and CaO. Additionally, the CaO clusters with n=4 and n=2 also demonstrated significant stability. These findings allow us to focus on studying the dehydration energy for thermochemical storage using these stable clusters. By understanding the stability and dehydration properties of these clusters, we can optimize the energy storage process, potentially enhancing the efficiency and effectiveness of $Ca(OH)_2$/CaO-based energy storage systems. This research paves the way for developing more reliable and durable materials for advanced thermochemical energy storage applications.

4.3 Defect energy

When calcium oxide (CaO) and calcium hydroxide ($Ca(OH)_2$) are doped with lithium (Li), the term "defect energy" refers to the energy required to insert lithium atoms into the crystal lattices

of the host material, either by replacing calcium atoms or occupying interstitial sites. The structural, electrical, and chemical properties of the materials are impacted by this process.

We determined the formation energy (E_f) for replacing a calcium atom with a lithium atom using the following equation

$$E_f = E_{defect} - E_{perfect} + \mu O - \mu Li \quad (19)$$

Here, E_{defect} represents the total energy of the $Ca(OH)_2$ and CaO cluster with one calcium atom substituted by a lithium atom, $E_{perfect}$ denotes the total energy of the perfect $Ca(OH)_2$ and CaO cluster, and μCa, μO and μLi are the chemical potentials of the calcium, Oxygen and lithium atoms, respectively. Also, to determine the formation energy of a lithium vacancy and interstitial in $Ca(OH)_2$ and CaO we apply the equation (20) and (21) respectively.

$$E_f = E_{defect} - E_{perfect} + \mu Li \quad (20)$$

$$E_f = E_{defect} - E_{perfect} - \mu Li \quad (21)$$

$$\mu_{Li} = {}_{1/2}E_{Li}, \ \mu_{Ca} = \tfrac{1}{4} E_{Ca} \text{ and } \mu_O = \tfrac{1}{2} E_O \quad (22)$$

Li-subs-Ca(OH)2	Cluster_size	E_f [eV]	Li-subs-CaO	Cluster_size	E_f [eV]	Li-i-Ca(OH)2	Cluster_size	E_f [eV]
	2	3.18		2	2.29		1	-0.54
	3	3.03		3	1.94		2	-0.49
	4	3.41		4	3.18		3	-0.84
	5	3.75		5	2.13		4	-0.82
	6	3.74		6	3.07		5	-0.5
	7	3.74		7	3.06		6	-0.31
	8	3.51		8	3.78		7	-0.58
	9	3.89		9	12.91		8	-0.61

	10	3.29		10	8.18		9	3.28
							10	2.9

Li_2-subs-Ca(OH)2	**Cluster_size**	**E_f [eV]**	**Li_2-subs-CaO**	**Cluster_size**	**E_f [eV]**	**Li-i-CaO**	**Cluster_size**	**E_f [eV]**
	2	-2.57		2	-1.24		1	-1.21
	3	-2.72		3	-2.10		2	-0.02
	4	-2.59		4	-0.49		3	-0.83
	5	-2.25		5	-2.35		4	-0.18
	6	-1.86		6	-1.05		5	-1.16
	7	-2.04		7	-1.71		6	0.67
	8	-2.08		8	-0.80		7	1.87
	9	-1.68		9	8.77		8	1.2
	10	-1.26		10	4.28		9	8.88
							10	6.17

Table 3: Computed Defect Energies of $Ca(OH)_2$ and CaO Clusters Doped with Lithium Atoms

4.4 Dehydration Energy of $Ca(OH)_2$ for Thermochemical Energy Storage

Dehydration energy refers to the energy required to remove water molecules from a hydrated compound. In the context of calcium hydroxide ($Ca(OH)_2$), dehydration involves converting it into calcium oxide (CaO) and water (H_2O). This process is essential for thermochemical energy

(storage applications, where energy is stored during the dehydration reaction and released during the rehydration reaction. [25]

We determine dehydration energy of calcium hydroxide ($Ca(OH)_2$) and calcium oxide (CaO) with cluster n= 6 for both clusters and n= 2,4 for CaO using the equation

$$E_{dehydration} = E_{CaO} + E_{H_2O} - E_{Ca(OH)_2} \quad (18)$$

$$Ca[(OH)_2]_6 \rightleftharpoons (CaO)_6(s) + 6H_2O(g)$$

$$E_{dehd\ Ca[(OH)_2]6} = E_{(CaO)6} + 6E_{H2O(g)} - E_{Ca(OH)_2}$$

$$= -42.984\ eV + 6(-12.213\ eV) - (-127.455\ eV) = 11.19\ eV$$

$$Ca[(OH)_2]_6 \rightleftharpoons (CaO)_4(s) + (CaO)_2 + H_2O(g)$$

$$= -83.283\ eV + -39.980\ eV + 6(-12.213\ eV) - (-127.455\ eV) = -69.09\ eV$$

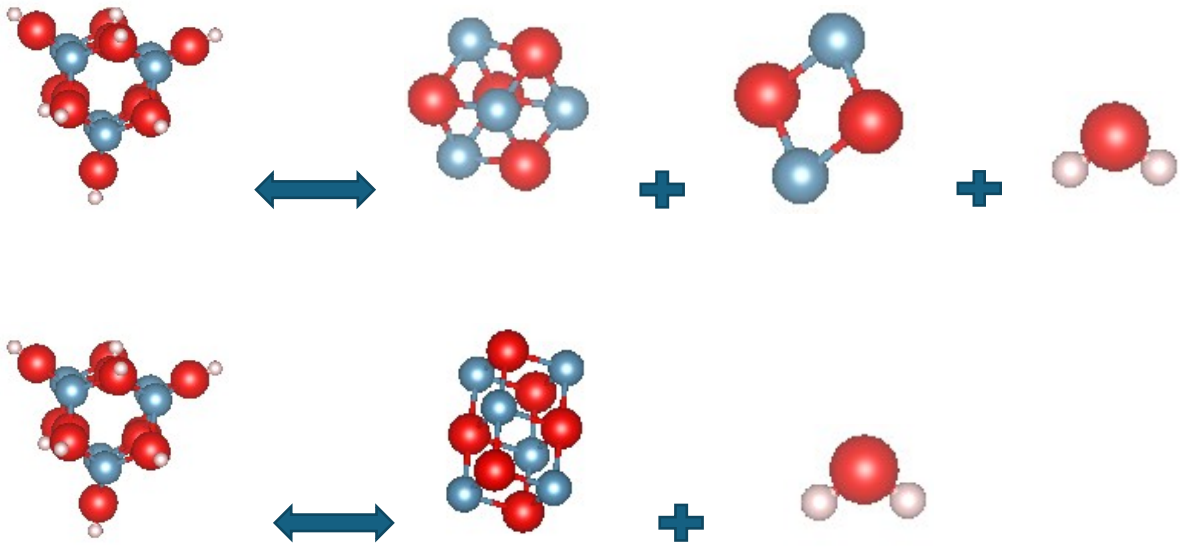

The negative dehydration energy for the n=6 cluster of $Ca(OH)_2$, calculated using Density Functional Theory (DFT), indicates that the dehydration reaction is exothermic. During this process, calcium hydroxide ($Ca(OH)_2$ decomposes into calcium oxide (n=6 CaO) and water (H_2O), releasing energy in the form of heat. In contrast, the positive dehydration energy for the decomposition of $Ca(OH)_2$ n=6 into CaO (n=4 and n=2) and water signifies that these reactions absorb heat during dehydration and release heat during hydration. This property makes them suitable for applications such as heat batteries and thermal energy storage systems.

4.4.1 Dehydration curve of p[H2O] vs Temperature plot of pure $Ca(OH)_2$/CaO clusters

Our study explored the dehydration reactions of calcium hydroxide ($Ca(OH)_2$ to form calcium oxide (CaO) clusters and release water (H_2O). We examined the following reactions under different temperature and pressure conditions: the dehydration of a single, two, three, four, five, or six units of $Ca(OH)_2$. We also studied an alternative reaction where six units dehydrate to form two separate clusters and six H_2O molecules. For each reaction, we plotted the logarithm of the water vapor pressure as a function of temperature to visualize the equilibrium shifts under varying thermal conditions and gain insights into the temperature and pressure dependencies of the dehydration processes for different cluster sizes.

Our analysis of these curves provided valuable insights into the thermodynamics of $Ca(OH)_2$ dehydration, which are essential for optimizing conditions for thermochemical energy storage. By identifying the most stable configurations and energy requirements for different cluster sizes, we contribute to the development of more efficient and reliable $Ca(OH)_2$/CaO-based energy storage systems that can operate under various environmental conditions while maintaining high stability and performance.

We plotted the curve of the water vapor pressure ($p[H_2O]$) as a function of temperature (in Kelvin) for the dehydration reactions mentioned above, as illustrated in Figure 11, below.

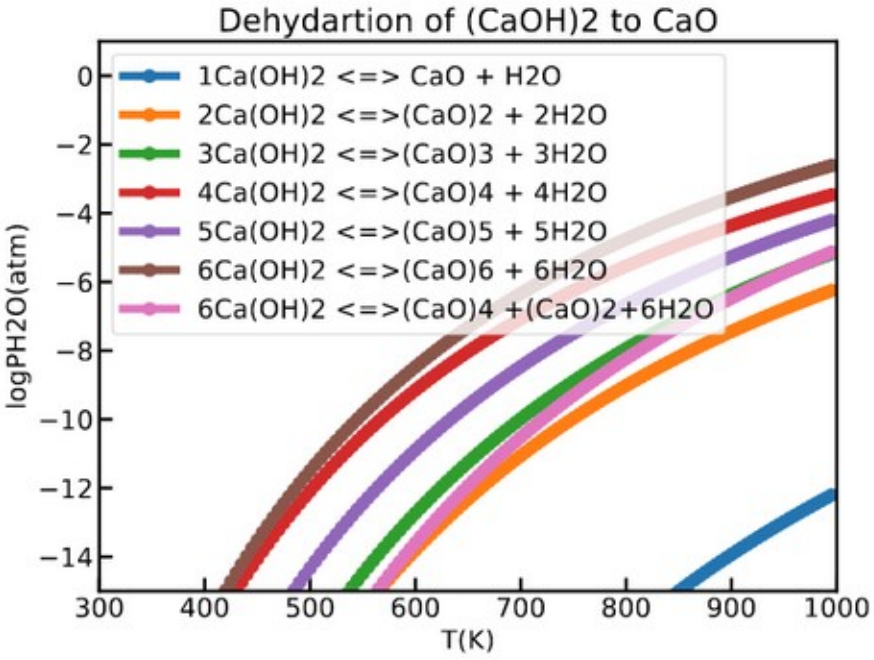

Fig.11, Equilibrium water vapor pressures vs temperature for the dehydration reactions of the $Ca(OH)_2$

Calcium hydroxide ($Ca(OH)_2$) undergoes dehydration at temperatures exceeding 425 K. At this temperature threshold, $Ca(OH)_2$ loses water molecules, transforming into calcium oxide (CaO) and water vapor (H_2O). For a single unit of $Ca(OH)_2$, represented by the cluster size of n = 1, the dehydration process occurs at a significantly higher temperature of 876 K. This higher temperature requirement indicates that smaller clusters have greater stability and require more energy to undergo dehydration.

In contrast, for larger cluster sizes, represented by n = 6, which comprises six units of $Ca(OH)_2$, the dehydration process occurs at a lower temperature of 430 K. This lower temperature requirement for dehydration suggests that larger clusters are less thermally stable than smaller ones and therefore require less energy to dehydrate. The presence of a low-temperature dehydration curve indicates that the equilibrium state favors the hydrated form, $Ca(OH)_2$, over the dehydrated form, CaO. This preference for the hydrated state is advantageous for energy storage applications because it implies that the material can remain in its hydrated form under relatively mild conditions, ensuring stable and predictable storage. Such stable storage conditions are essential for the long-term reliability of thermochemical energy storage systems.

Maintaining the hydrated state at lower temperatures ensures that the material does not prematurely dehydrate, which could lead to energy loss and reduced efficiency of the storage system. Therefore, the ability to maintain a hydrated state under predictable conditions contributes to the overall long-term stability and effectiveness of the $Ca(OH)_2$/CaO energy storage system, making it a viable option for sustainable and efficient thermal energy storage solutions.

Conclusion

The cluster of CaOn/[$Ca(OH)_2$]n was produced using the ABcluster tool and the structures were optimized using the VASP (Vienna Ab-initio Simulation Package) software. This approach allowed for systematic generation and optimization of the cluster structures.

The binding energy, formation energy, and relative stability of the different cluster isomers were calculated. These energetic parameters were essential in determining the most stable isomer configurations among the CaOn/[$Ca(OH)_2$]n clusters.

Furthermore, the dehydration curve was plotted as a function of temperature. This provided insights into the thermal behavior and decomposition of the calcium hydroxide clusters. Additionally, the defect energy formation of vacancy, substitution, and interstitial defects was calculated for the clusters.

Based on the comprehensive analysis of the structural, energetic, and thermal properties, a $CaO/Ca(OH)_2$ cluster with n=6 was selected as the most promising candidate for further investigation in energy storage applications. The detailed understanding of this optimized cluster structure and its characteristics will inform the development of improved calcium-based energy storage materials and systems.

In summary, the systematic approach of cluster generation, optimization, and multi-faceted analysis enabled the identification of a stable and promising CaO/Ca(OH)2 cluster configuration for energy storage applications. This work highlights the valuable insights that can be gained through the integration of computational materials modeling and experimental investigations.

Reference

1. Experimental and Numerical Investigation of the Dehydration of $Ca(OH)_2$ at Low Steam Pressures *Processes* **2022**, *10*(2), 325; https://doi.org/10.3390/pr10020325

2. Yi Yuan, Yingjie Li, Lunbo Duan, Hantao Liu, Jianli Zhao, Zeyan Wang,CaO/Ca(OH)2 thermochemicalheat storage of carbide slag from calcium looping cycles for CO2 capture,EnergyConversion and Management,Volume 174,2018,Pages 8-19,

3. Kyriaki G. Sakellariou, George Karagiannakis, Yolanda A. Criado, Athanasios G. Konstandopoulos,Calcium oxide based materials for thermochemical heat storage inconcentrated solar power plants,Solar Energy,Volume 122,2015,Pages 215-230,ISSN 0038-092X,https://doi.org/10.1016/j.solener.2015.08.011.

4. Prieto C, Cooper P, Fernández AI, Cabeza LF. Review of technology: Thermochemical energy storage for concentrated solar power plants. Renew. Sustain. Energy Rev. 2016;60:909–29.452 doi:10.1016/j.rser.2015.12.364.

5. Funayama, S., Takasu, H., Zamengo, M., Kariya, J., Kim, S. T., & Kato, Y. (2019). *Composite Material for High-Temperature Thermochemical Energy Storage using Calcium Hydroxide and Ceramic Foam. Energy Storage, e53.* doi:10.1002/est2.53

6. M.N. Azpiazu, J.M. Morquillas, A. Vazquez,Heat recovery from a thermal energy storagebased on the Ca(OH)2/CaO cycle,Applied Thermal Engineering,Volume 23, Issue 6,2003,Pages 733-741,ISSN 1359-4311,https://doi.org/10.1016/S1359-4311(03)00015-2.

7. Wu QP. (2022). Superior Performance of Ca(OH)2-CaO-H2O System Doped with Cerium and Lithium for Thermochemical Energy Storage. Catal Res. 2(1):02.

8. Shkatulov A, Aristov Y. (2015). Modification of magnesium and calcium hydroxides with salts: An efficient way to advanced materials for storage of middle-temperature heat. Energy. 85:667-676.

9. Yan J, Zhao CY. (2014). First-principle study of CaO/Ca(OH)2 thermochemical energy storage system by Li or Mg cation doping. Chem Eng Sci. 117:293-300.

10. Zhang, J.; Dolg, M. Phys. Chem. Chem. Phys. 2015, 17, 24173– 40824181.

11. Malloum, A., Fifen, J. J., Dhaouadi, Z., Nana Engo, S. G., & Conradie, J. (2019). Structures, Relative Stabilities and Binding Energies of Neutral Water Clusters, (H2O)2-30. New Journal of Chemistry

12. Guangyu Sun, Jenö Kürti, Péter Rajczy, Miklos Kertesz, Jürgen Hafner, Georg Kresse,Performance of the Vienna ab initio simulation package (VASP) in chemical pplications,Journal of Molecular Structure: THEOCHEM,Volume 624, Issues 1–3,2003,Pages 37-45,ISSN 0166-1280,https://doi.org/10.1016/S0166-1280(02)00733-9.

13. Wencai Yi, Gang Tang, Xin Chen, Bingchao Yang, Xiaobing Liu,qvasp: A flexible toolkit for VASP users in materials simulations,Computer Physics Communications,Volume 257,2020,107535,ISSN 0010-4655,https://doi.org/10.1016/j.cpc.2020.107535.

14. R. Sun, Z. Wang, M. Saito, N. Shibata, Y. Ikuhara, Nature Commun. 6 (2015)7120.

15. Z. Guo, Y. Li, B. Sa, Y. Fang, J. Lin, Y. Huang, C. Tang, J. Zhou, N. Miao, Z.Sun, Appl. Surf. Sci. 521 (2020) 146436.

16. Panyu Zhang *et al* 2023 *J. Electrochem. Soc.* **170** 060547

17. P. Hohenberg and W. Kohn, Phys. Rev., 136,B864 (1964).Inhomogeneous Electron Gas.

18. Bartolotti, L. J., & Flurchick, K. (2007). An Introduction to Density Functional Theory. Reviews in Computational Chemistry, 187–216. doi:10.1002/9780470125847.ch4 10.1002/9780470125847.ch4

19. J. Kendrick and M. Fox,]. Mol. Graphics, 9, 182 (1991).Calculation and Display of Electro-static Potentials.

20. Yan, J., & Zhao, C. Y. (2014). First-principle study of CaO/Ca(OH)2 thermochemical energy storage system by Li or Mg cation doping. Chemical Engineering Science, 117, 293–300. doi:10.1016/j.ces.2014.07.007

21. Darkwa, K., O'Callaghan, P.W., 1997. Analytical studies of a thermochemical store for minimising energy consumption and air pollution from automobile engines. Appl. Ther. Eng. 17, 603–614.

22. Carrasco, J., Illas, F., Lopez, N., 2008. Dynamic Ion pairs in the adsorption of isolatedwater molecules on alkaline-earth oxide (001) surfaces. Phys. Rev. Lett. 11 (016101-1 - 016101-4).

23. QuantumATK Case Studies.com

24. Wu, L., Dong, Y., Springborg, M., Zhang, L., & Qi, Y. (2015). Study of structure, energy, and electronic properties of small-sized Si x Ge y (x + y = 2–8) alloy clusters based on density functional tight binding calculations. Computational and Theoretical Chemistry, 1074, 185–193. doi:10.1016/j.comptc.2015.10.022

25. Criado, Y. A., Alonso, M., & Abanades, J. C. (2014). Kinetics of the CaO/Ca(OH)2 Hydration/Dehydration Reaction for Thermochemical Energy Storage Applications. Industrial & Engineering Chemistry Research, 53(32), 12594–12601. doi:10.1021/ie404246p
26. Sun, F.; Peng, H.; Ling, X. Progress in Medium to High Temperature Thermochemical Energy Storage Technologies. Energy Storage Sci. Technol. 2015, 4, 577–584
27. Yan, J.; Zhao, C.Y. Experimental Study of CaO/Ca(OH)2 in a Fixed-Bed Reactor for Thermochemical Heat Storage. Appl. Energy 2016, 175, 277–284.
28. Linder, M.; Roßkopf, C.; Schmidt, M.; Wörner, A. Thermochemical Energy Storage in kW-scale Based on CaO/Ca(OH)2. Energy Procedia 2014, 49, 888–897
29. Sakellariou, K.G.; Karagiannakis, G.; Criado, Y.A.; Konstandopoulos, A.G. Calcium Oxide Based Materials for Thermochemical Heat Storage in Concentrated Solar Power Plants. Sol. Energy 2015, 122, 215–230
30. Knoll, C.; Müller, D.; Artner, W.; Welch, J.M.; Werner, A.; Harasek, M.; Weinberger, P. Probing Cycle Stability and Reversibility in Thermochemical Energy Storage-CaC2O4·H2O as Perfect Match? Appl. Energy 2017, 187,1–9
31. Azpiazu, M.N.; Morquillas, J.M.; Vazquez, A. Heat Recovery From a Thermal Energy Storage Based on the Ca(OH)2/CaO Cycle. Appl. Therm. Eng. 2003, 23, 733–741
32. Yan, J.; Zhao, C.Y. Thermodynamic and Kinetic Study of the Dehydration Process of CaO/Ca(OH)2 Thermochemical Heat Storage System with Li Doping. Chem. Eng. Sci. 2015, 138, 86–92

APPENDIX 1 $Li(Ca_{n-1}OH)_n$ low-lying isomers

	$Li(Ca_{n-1}OH)_n$	**$LiCa_{n-1}O_n$**
n=2	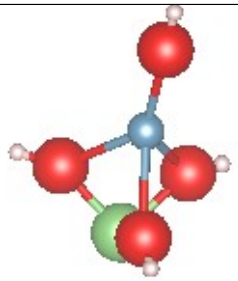 **-38.796 eV** 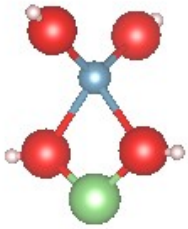 **-38.673 eV** 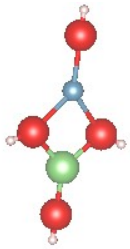 **-38.340 eV** 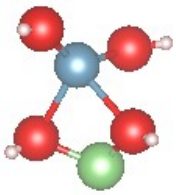 **-38.362 eV**	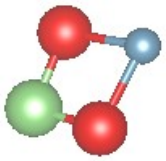 **-10.505 eV** 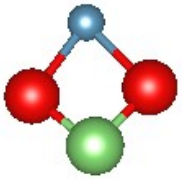 **-10.502 eV**

n=3	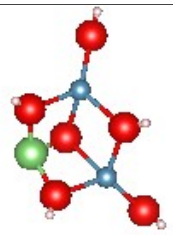 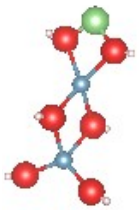 **-60.325 eV** **-59.941 eV** 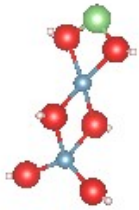 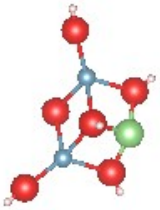 **-60.279 eV** **-60.1551 eV**	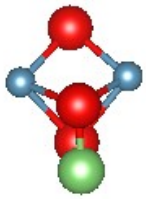 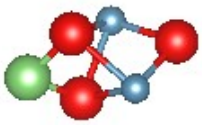 **-17.801 eV** **-17.802 eV** 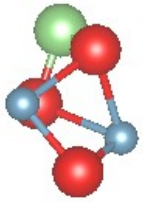 **-17.801 eV**
n=4	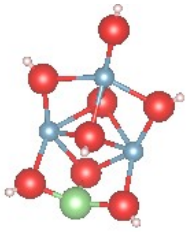 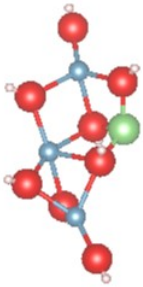 **-81.802 eV** **-81.589 eV** 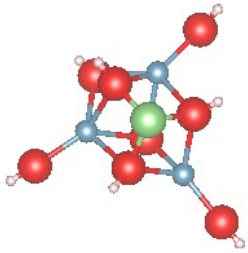 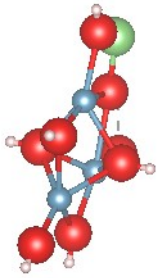 **-81.819 eV** **-81.591 eV**	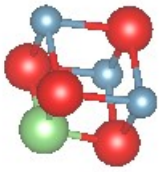 **-26.019 eV** 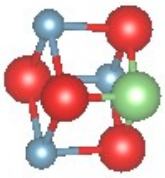 **-26.004 eV**

n=5	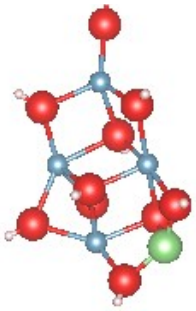 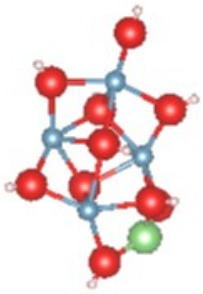 **103.621 eV** **-103.502 eV** 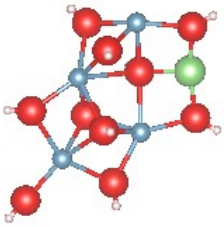 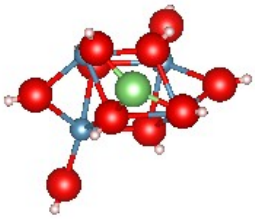 **103.577 eV** **-103.411 eV**	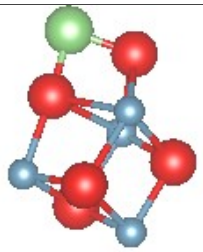 **-33.508 eV** 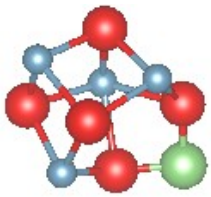 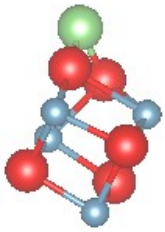 **-33.609 eV** **-33.497 eV**
n=6	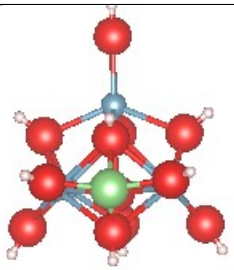 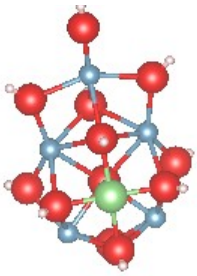 **-125.685 eV** **-125.390 eV** 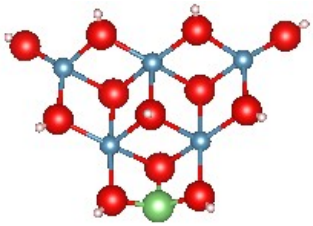 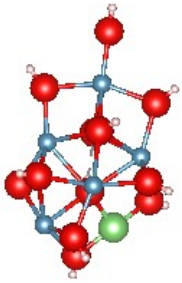 **125.547 eV** **-125.547 eV**	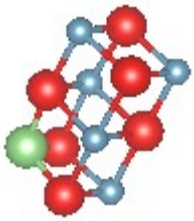 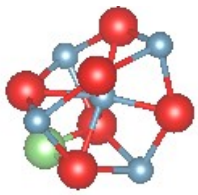 **-41.856 eV** **-40.707 eV** 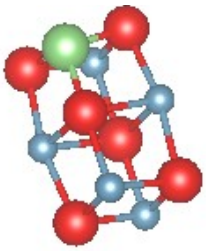 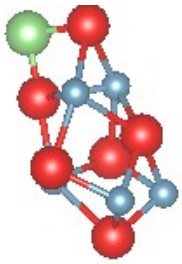 **-41.852 eV** **-38.411 eV**

	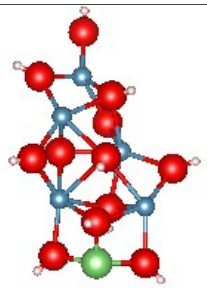 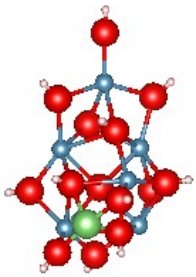 **125.198 eV** **-125.209 eV**	
n=7	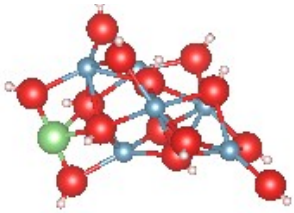 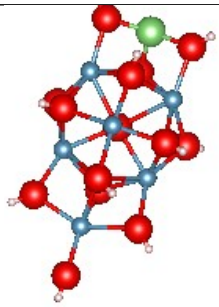 **-147.325 eV** **-147.298 eV** 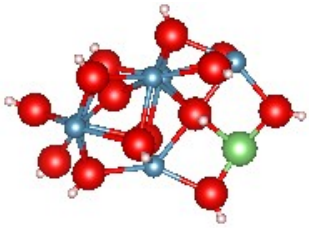 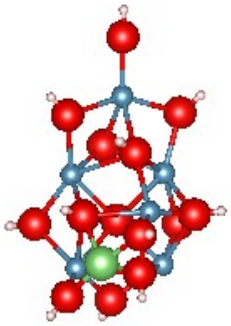 **-147.394eV** **-147.404 eV**	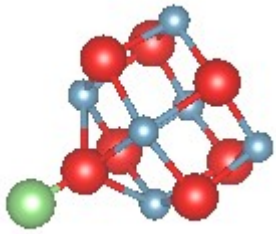 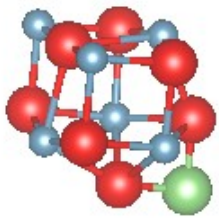 **-48.483 eV** **-48.860 eV** 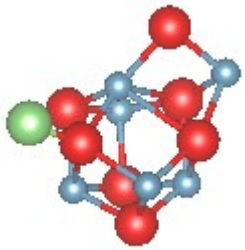 **-47.795 eV** 1Li-subs-CaO
n=8	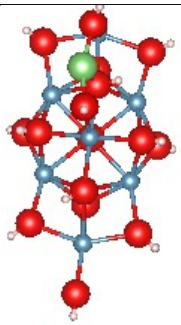 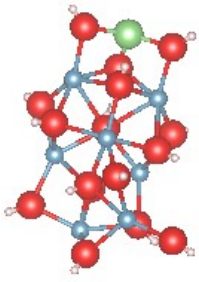 -	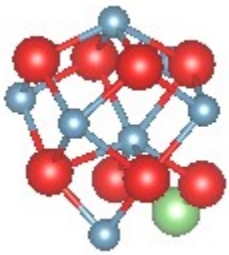 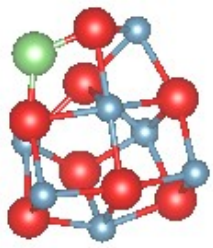

	169.260 eV **-169.498 eV** 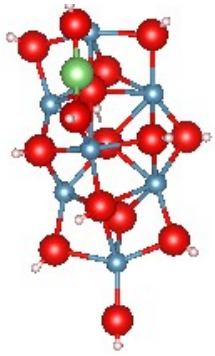 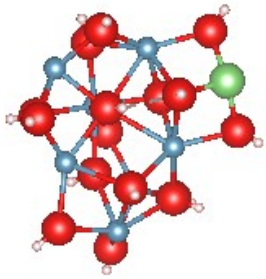 **169.498 eV** **-169.369 eV**	**-48.483 eV** **-48.860 eV** 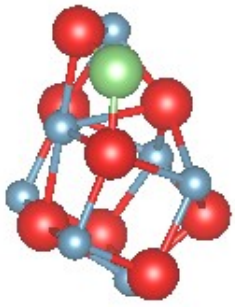 **-47.795 eV**
n=9	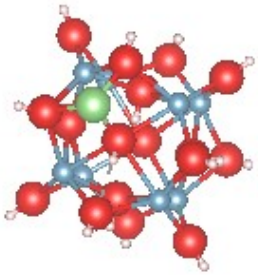 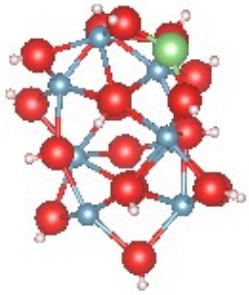 **-191.595 eV** **-191.417 eV** 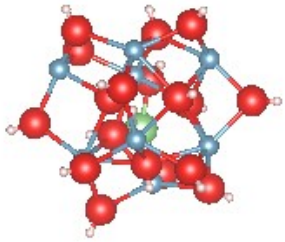 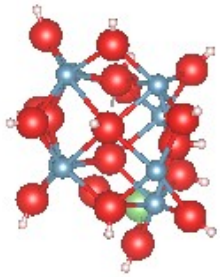 **-191.237 eV** **-191.099 eV**	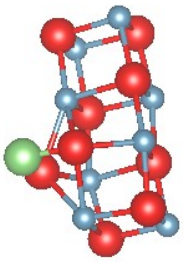 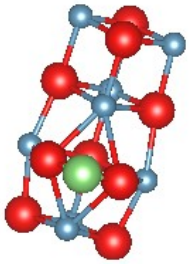 **-64.755eV** **-64.754 eV** 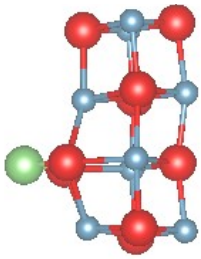 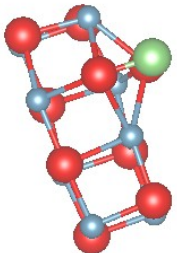 **-64.764 eV** **-64.766 eV**

n=10	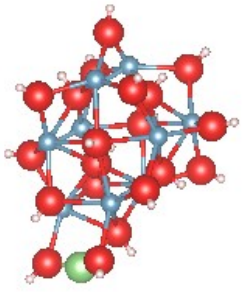 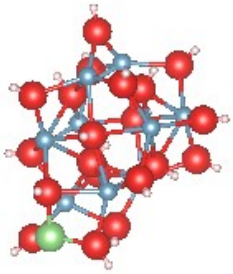 **-214.134 eV** **-213.744 eV** 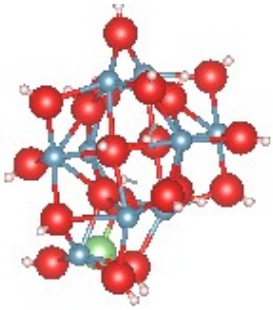 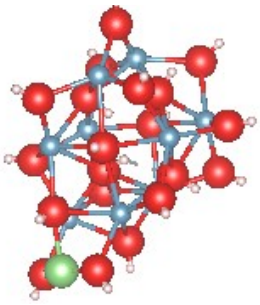 **-213.383 eV** **-213.507 eV**	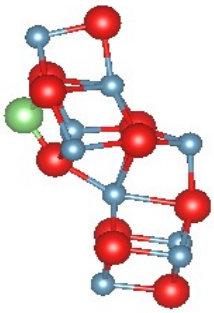 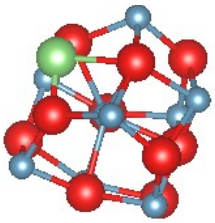 **-70.396 eV** **-72.244 eV** 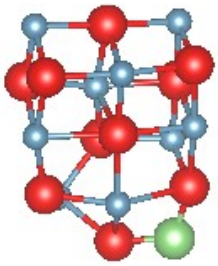 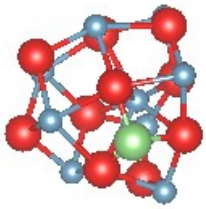 **-77.191 eV** **-77.030 eV**

APPENDIX 2

$Li_2(Ca_{n-1}OH)_n$ (n=2−10), $Li_2Ca_{n-1}O_n$ (n=2−10) And Li-i-Ca(OH)2, Li-i-CaO low-lying isomers

	$Li_2(Ca_{n-1}OH)_n$ (n=2−10)	**$Li_2Ca_{n-1}O_n$ (n=2−10)**
n=2	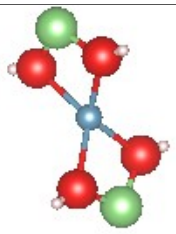 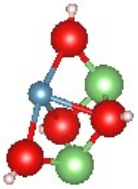 **-44.541 eV** **-44.172 eV** 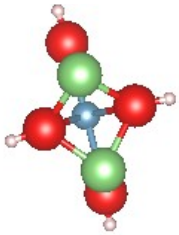 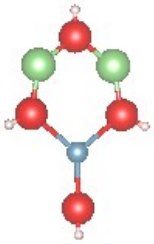 **-44.068 eV**	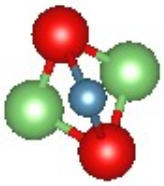 **-14.037 eV**
n=3	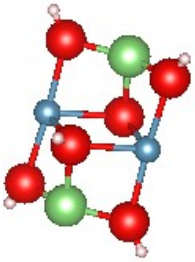 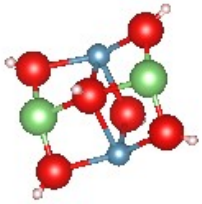 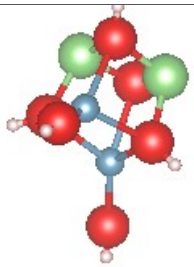 **-66.092 eV** **-65.951 eV** **-65.916 eV**	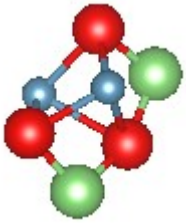 **-21.854 eV**

	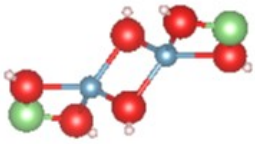 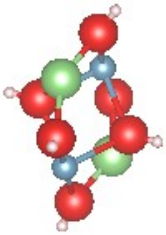 **-65.7937 eV** **-65.542 eV**	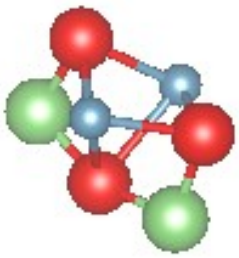 **-21.860 eV**
n=4	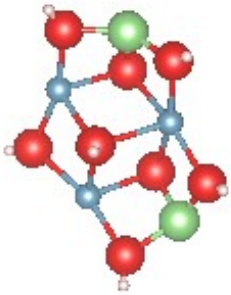 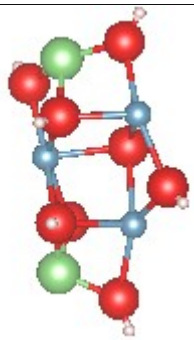 **87.810 eV** **-87.598 eV** 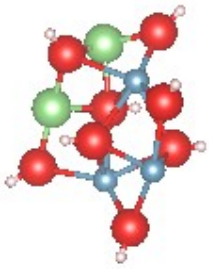 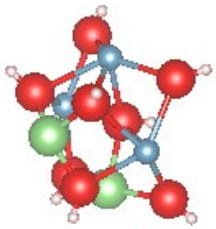 **87.585 eV** **-87.226 eV**	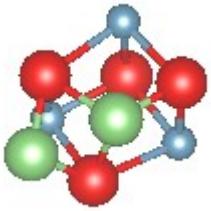 **-29.689 eV** 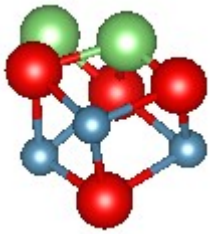 **-29.693 eV**
n=5	**-109.411 eV** **-109.587 eV**	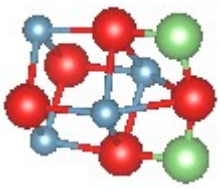 **-38.110 eV**

	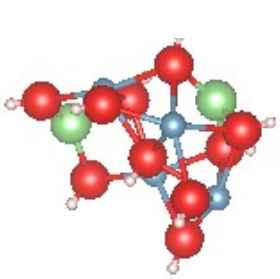 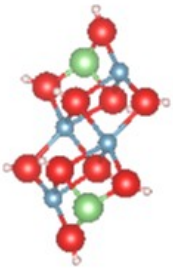 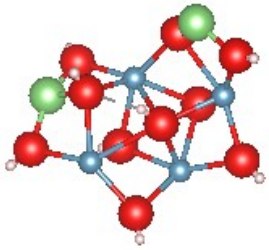 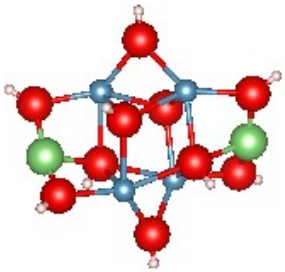 - **108.983 eV** **-109.218 eV** 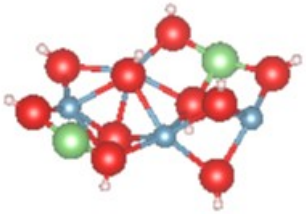 **-109.303 eV**	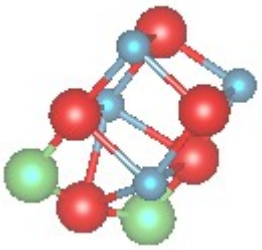 **-38.092 eV**
n=6	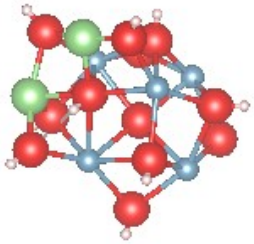 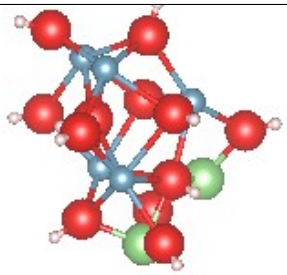 **-131.246 eV** **-131.197 eV**	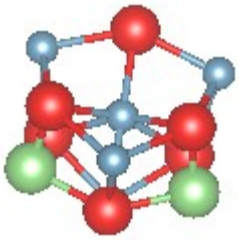 **-43.080 eV** 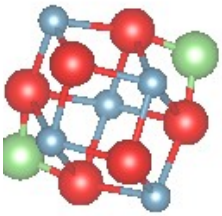 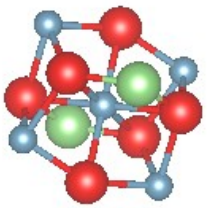 -

	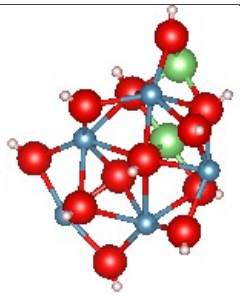 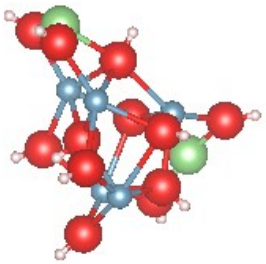 **131.197 eV** **-131.276 eV** 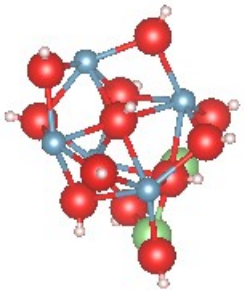 **-131.109 eV**	**45.532 eV** **-43.541 eV** 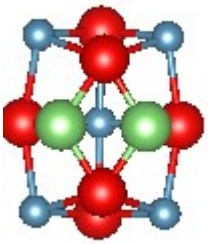 **-45.998 eV**
n=7	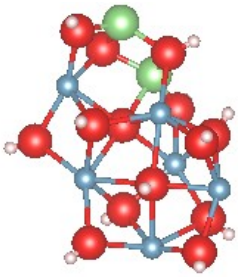 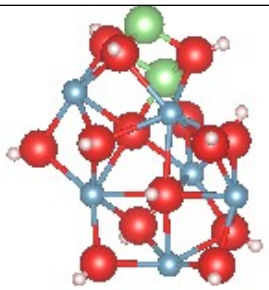 **153.163 eV** **-153.181 eV** 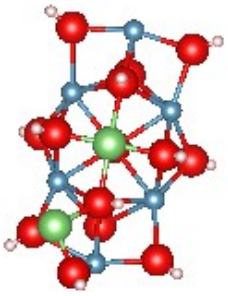 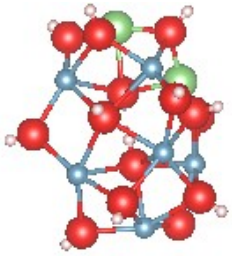 **153.070 eV** **-152.745 eV**	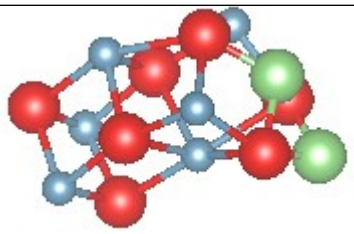 **-53.458 eV** 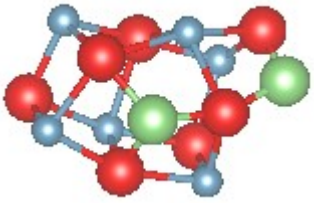 **-53.633 eV**

		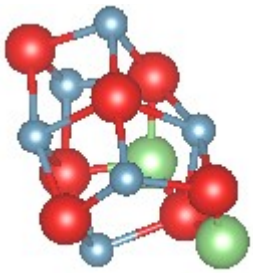 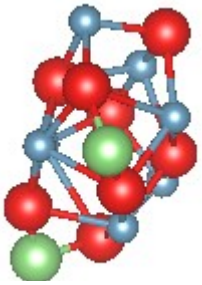 - **53.620 eV** **-53.452 eV**
n=8	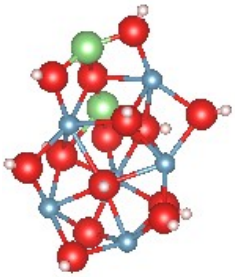 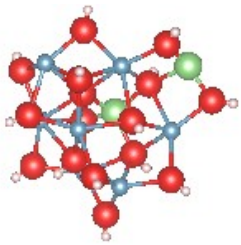 - **175.098 eV** **-174.924 eV** 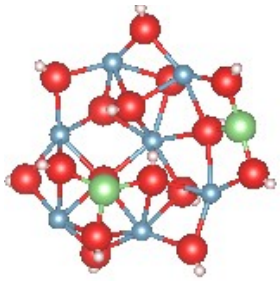 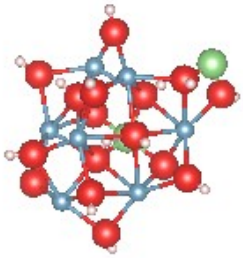 - **174.734 eV** **-174.441 eV**	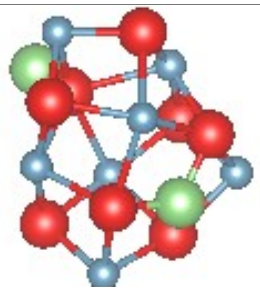 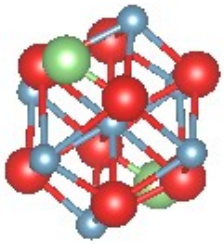 - **61.234 eV** **-59.965 eV** 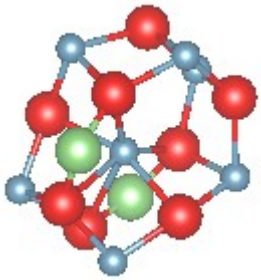 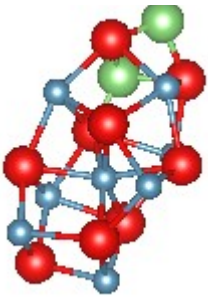 **-56.051 eV** **-61.071 eV**
n=9	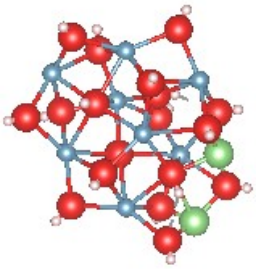 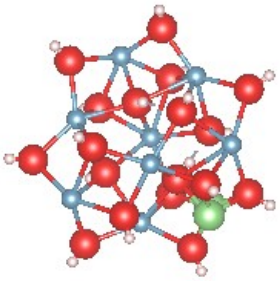 - **196.915 eV** **-196.981 eV**	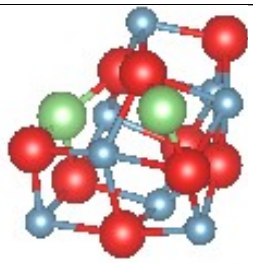 **-67.264 eV**

	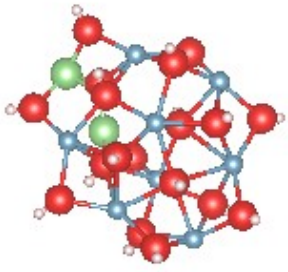 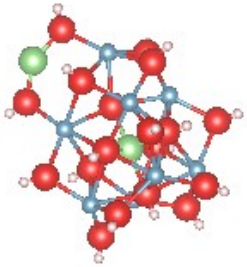 **196.651 eV** **-196.902 eV**	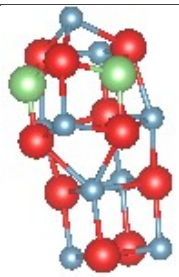 **-68.900 eV**
n=10	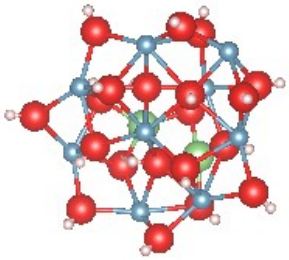 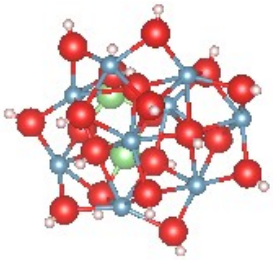 **218.761 eV** **-218.652 eV** 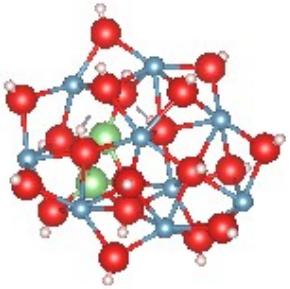 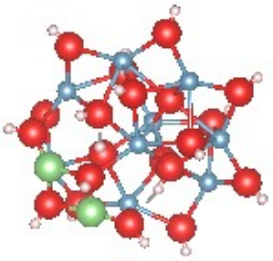 **218.502 eV** **-218.658 eV**	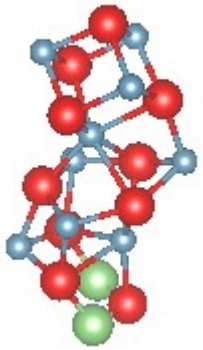 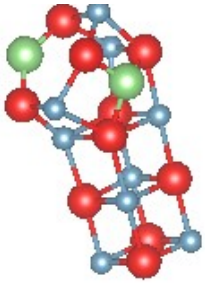 **-76.926 eV** **-75.182 eV** 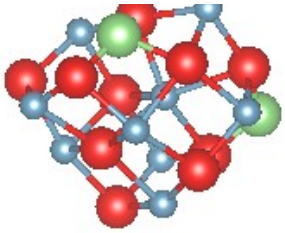 **-77.191 eV**
	Li-i- $(Ca(OH)_2)_n$	**Li-i-$(CaO)_n$**

n=1	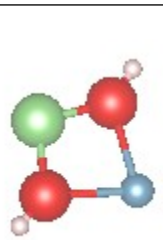 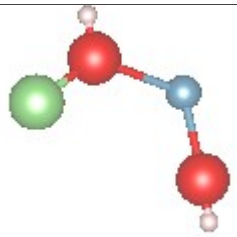 **-20.780 eV** **-19.866 eV**	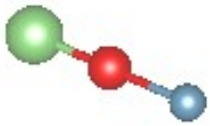 **-5.5511 eV**
n=2	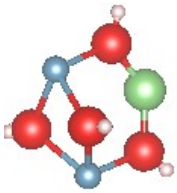 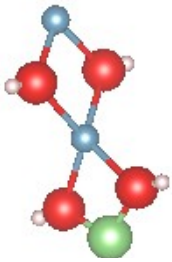 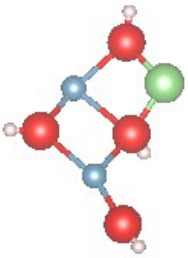 **-42.061 eV** **-42.033 eV** **-42.048 eV**	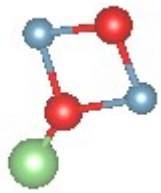 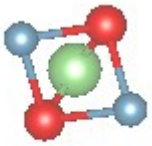 **-12.9521 eV** **-12.444 eV**
n=3	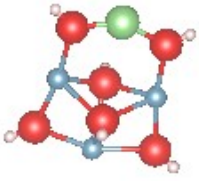 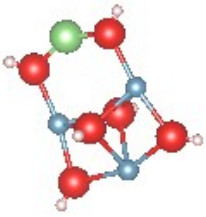 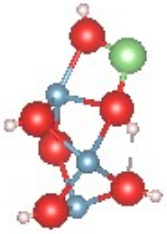 **-63.844 eV** **-63.799 eV** **-63.233 eV** 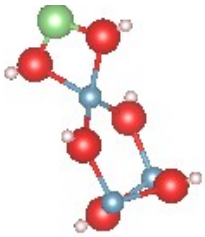 **-63.233 eV**	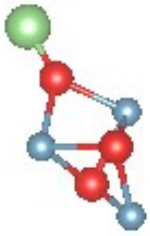 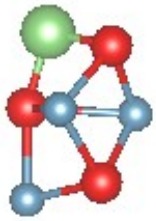 **-19.770 eV** **-20.212 eV**

n=4	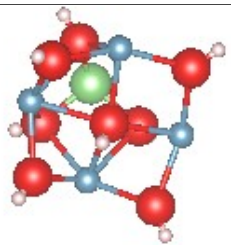 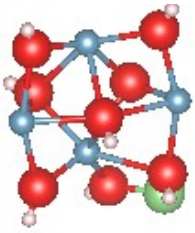 **-85.295** 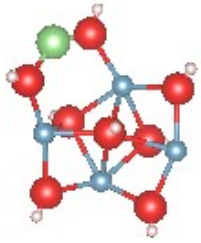 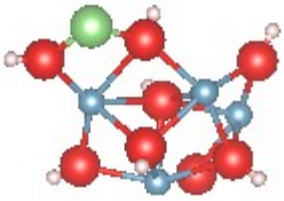 **-85.242 eV** **-85.299 eV**	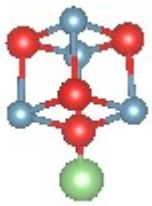 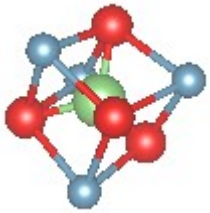 **-28.997 eV** **-26.420 eV** 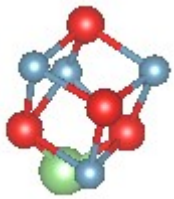 **-27.945 eV**
n=5	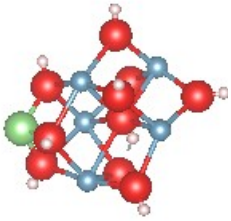 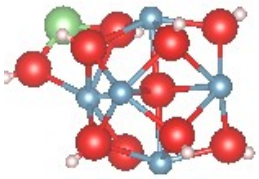 **-107.456 eV** **-107.339 eV** 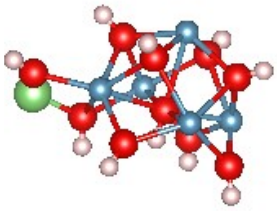 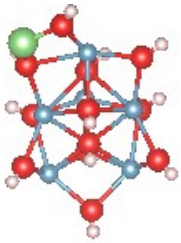 - **107.454 eV** **-107.200 eV**	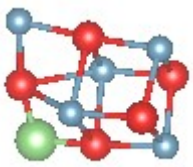 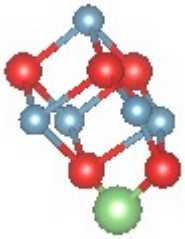 **-36.388 eV** **-36.518 eV**
n=6	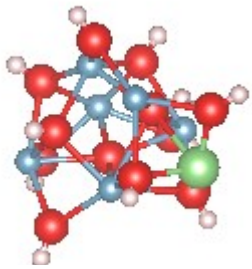 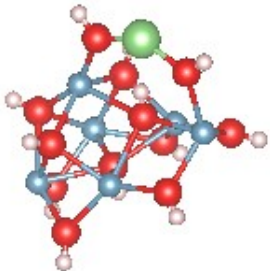 -	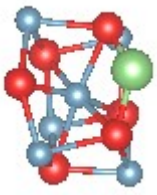 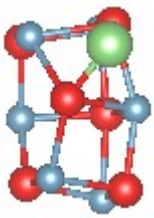

	129.206 eV **-129.184 eV** 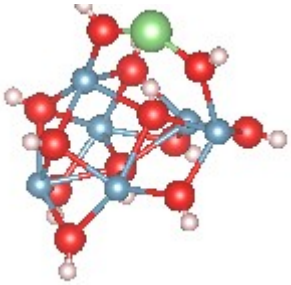 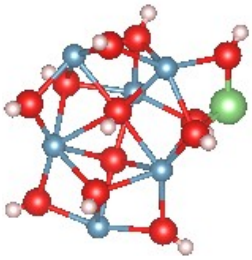 **129.250 eV** **-129.063 eV**	**-42.346 eV** **-43.910 eV**  **-43.901 eV**
n=7	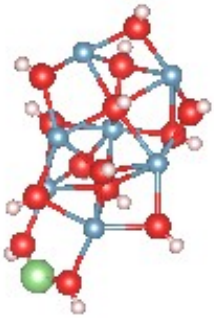 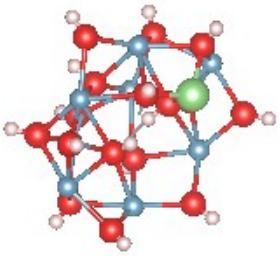 **150.983 eV** **-151.325 eV** 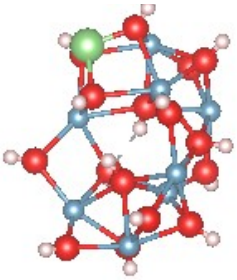 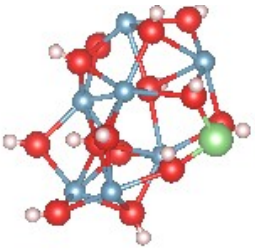 **151.094 eV** **-151.387 eV**	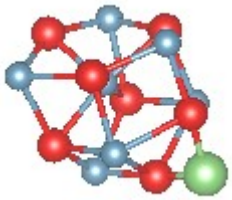 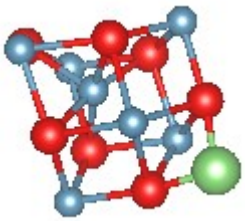 **-49.662 eV** **-49.655 eV** 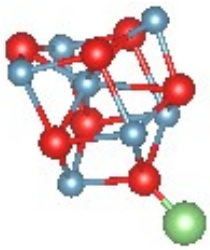 **-49.327 eV**
n=8	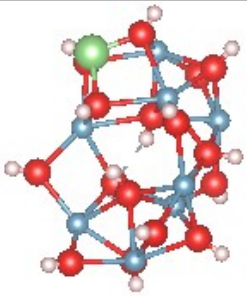 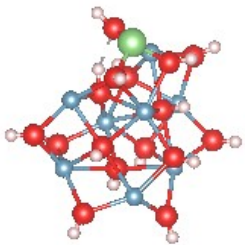 **173.252 eV** **-173.117 eV**	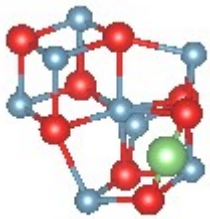 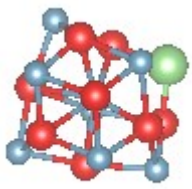 **59.192 eV** **-59.194 eV**

	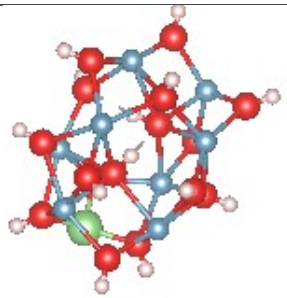 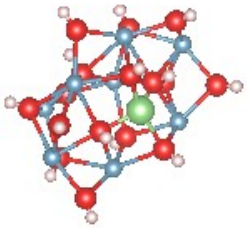 **173.235 eV** **-172.931 eV**	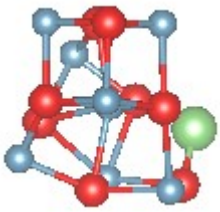 **-59.237 eV**
n=9	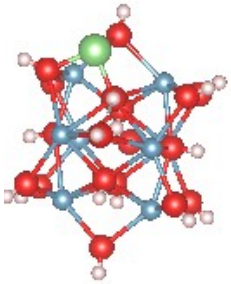 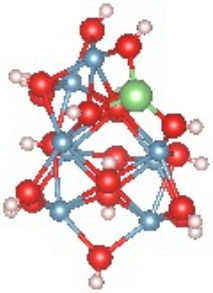 **-191.5989 eV** **-191.103 eV** 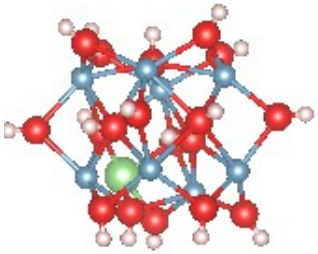 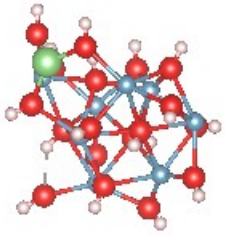 **190.998 eV** **-191.134 eV**	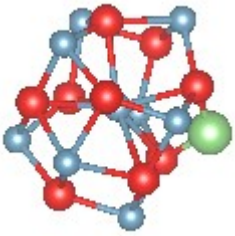 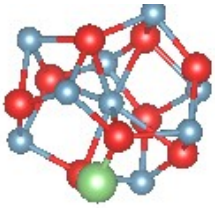 **-68.429 eV** **-68.452 eV** 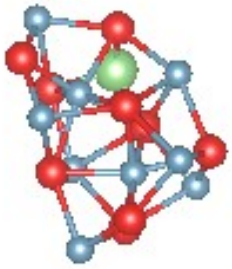 **-63.161 eV**
n=10	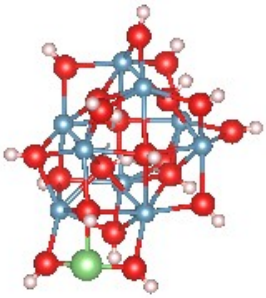 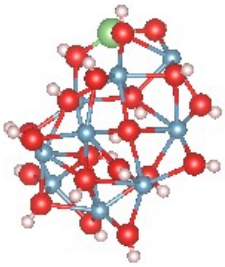 **213.499 eV** **-212.981 eV**	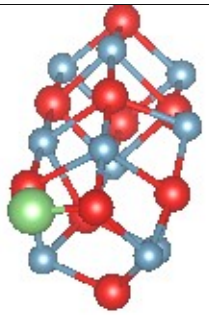 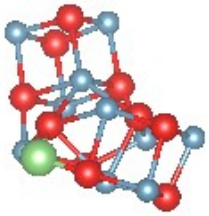 **-75.542 eV** **-74.783 eV**

	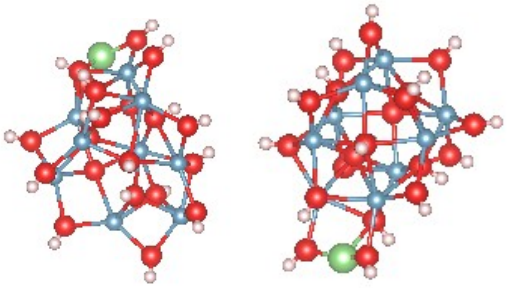 **-212.946 eV** **-214.129 eV**	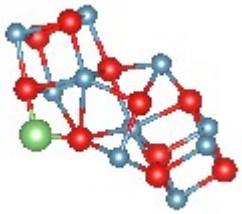 **-74.753 eV**
	$LiNO_3$- $(Ca(OH)_2)_n$	
n=1	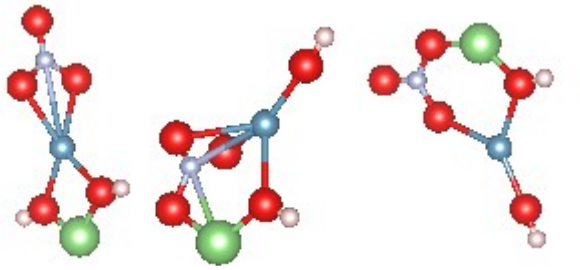 **-41.857 eV** **-41.227 eV** **-41.302 eV**	
n=2	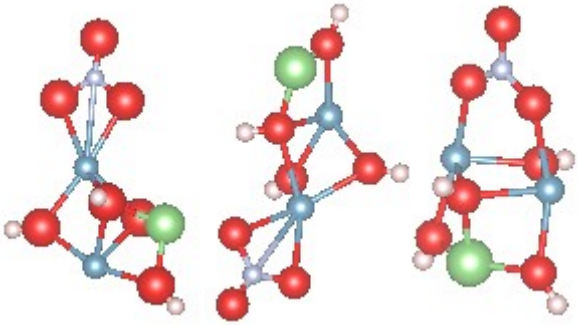 **-63.086 eV** **-62.984 eV** **-62.873 eV**	

n=3	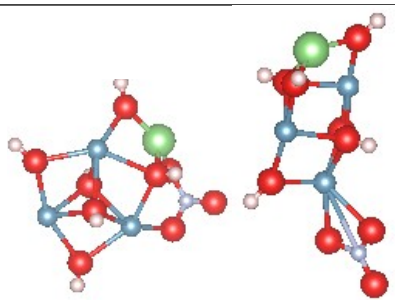 **-84.590 eV** **-85.009 eV** 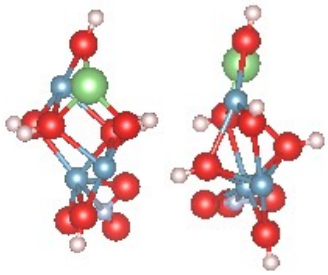 **-84.971 eV** **-84.587 eV**	
n=4	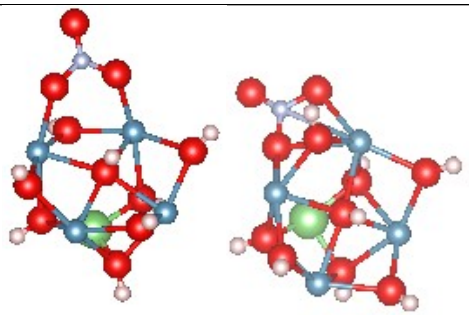 **-106.435 eV** **-106.372 eV** 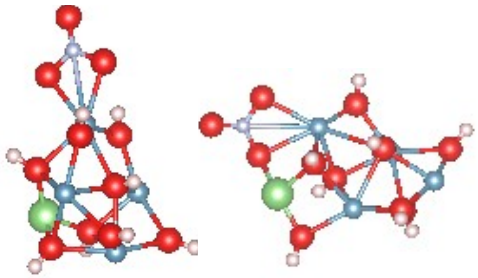	

	-106.394 eV **-106.387 eV**	
n=5	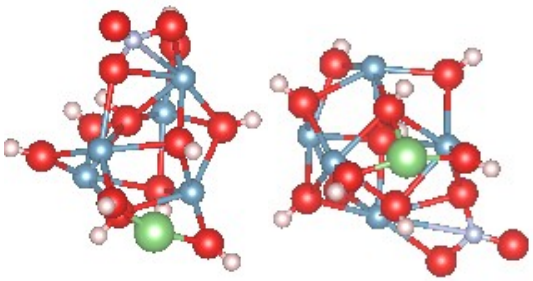 **-128.573 eV** **-128.564 eV** 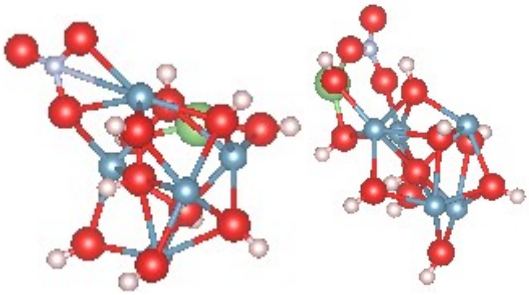 **-128.579 eV** **-128.579 eV**	
n=6	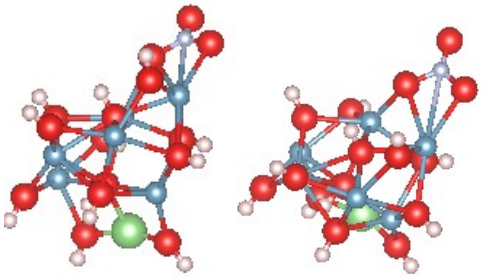 **-150.390 eV** **-150.382 eV**	

	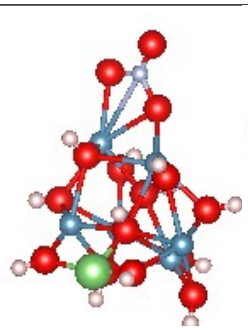 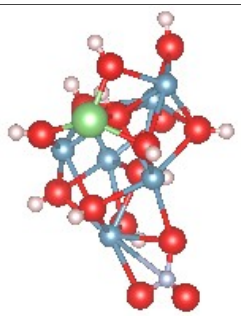 **-150.394 eV** **-150.384 eV**	
n=7	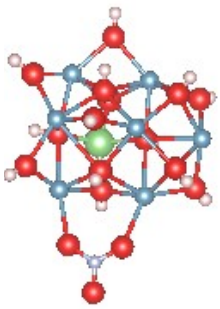 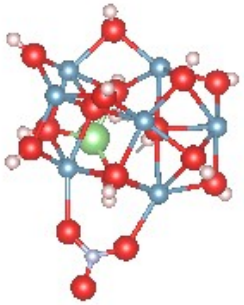 **-172.450 eV** **-172.178 eV** 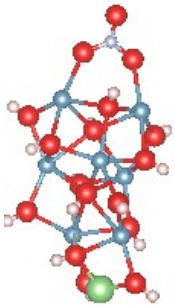 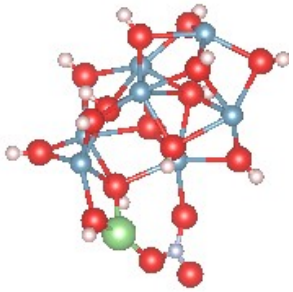 **-172.334 eV** **-171.962 eV**	

n=8	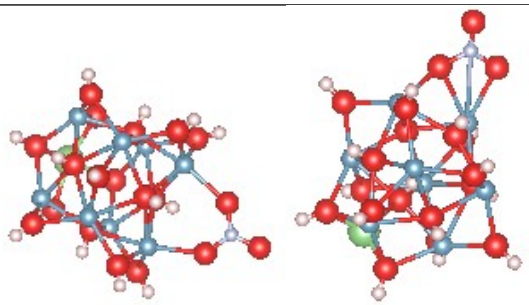 **-194.142 eV** **-194.429 eV** 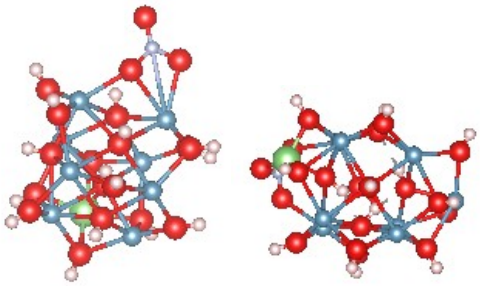 **-194.396 eV** **-193.639 eV**	
n=9	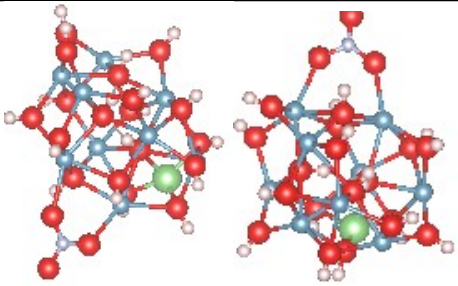 **-216.194 eV** **-215.761 eV** 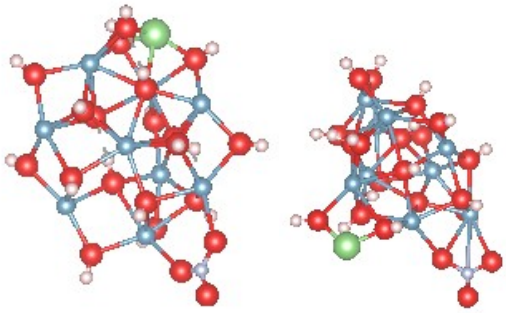	

	-215.878 eV **-215.752 eV**	
n=10	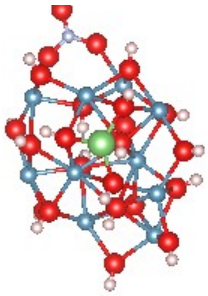 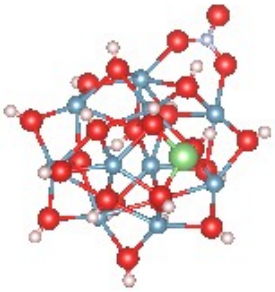 **-237.707 eV** **-237.814 eV** 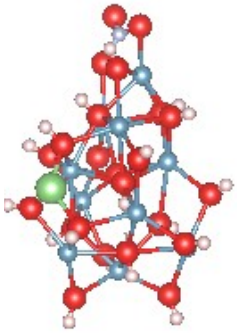 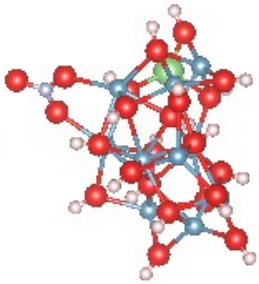 **-237.874 eV** **-237.631 eV**	
	$LiCl-(Ca(OH)_2)_n$	
n=1	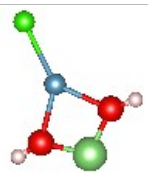 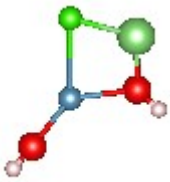 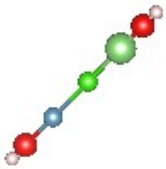 **-24.529 eV** **-24.296 eV** **-22.426 eV**	

n=2	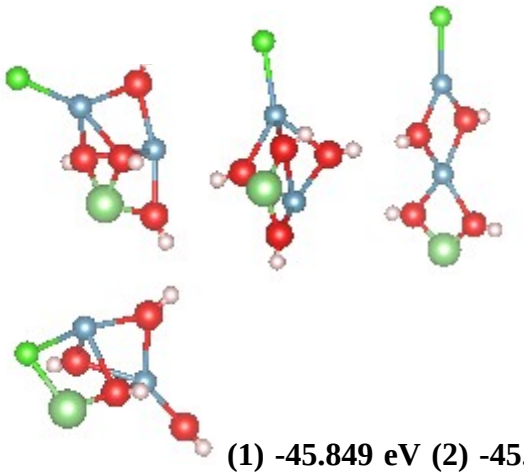 **(1) -45.849 eV (2) -45.720 eV (3) -45.780 eV (4) -45.449 eV**	
n=3	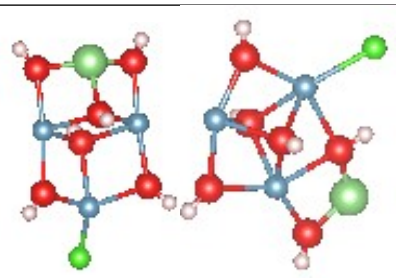 **-67.690 eV -67.258 eV** 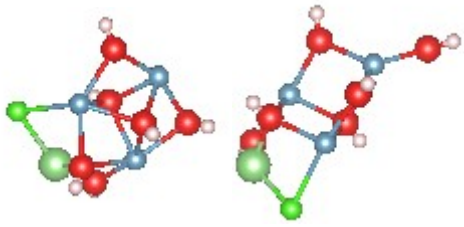 **-67.349 eV -67.477 eV**	
n=4	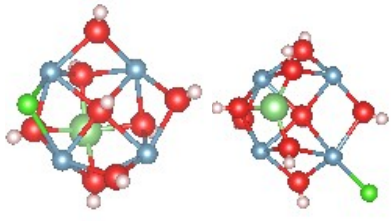	

	-89.119 eV **-89.135 eV** 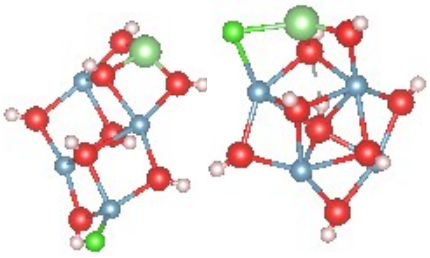 **-89.383 eV** **-89.086 eV**	
n=5	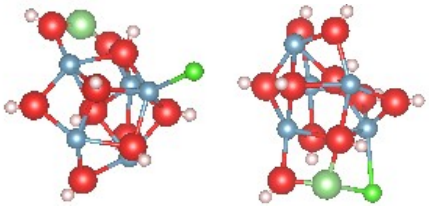 -111.267 eV -111.201 eV 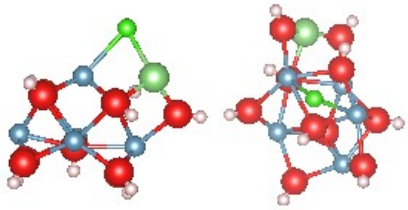 -111.154 eV -111.284 eV	
n=6	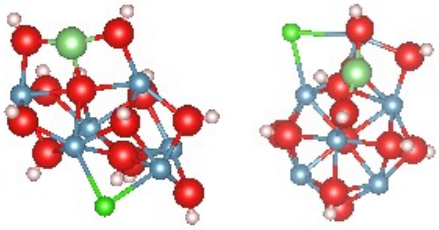 -133.182 eV -133.213 eV	

	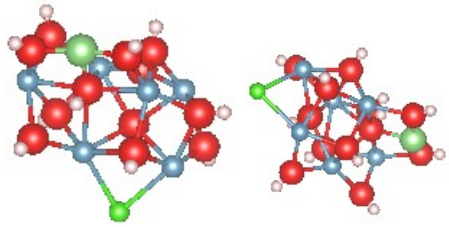 -133.178 eV -133.192 eV	
n=7	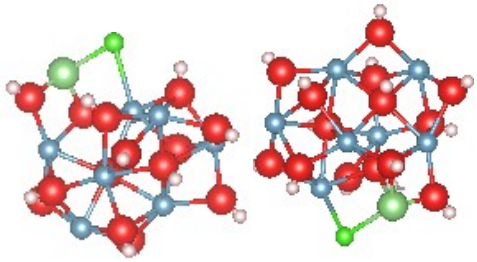 -177.094 eV -177.079 eV 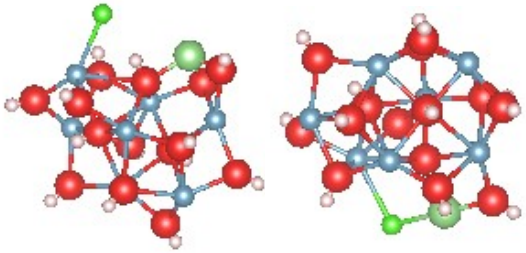 -176.994 eV -176.712 eV	
n=8	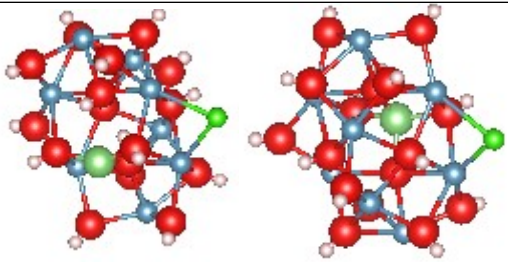 -177.094 eV -177.079 eV	

	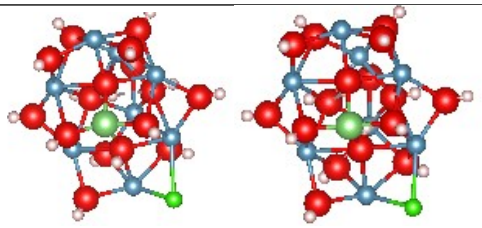 -176.994 eV -176.712 eV	
n=9	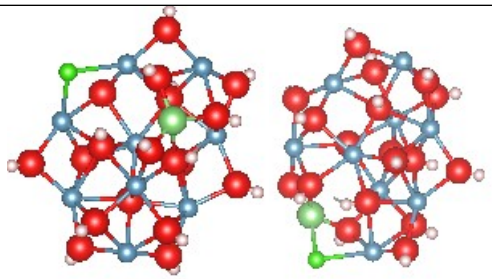 -199.075 eV -198.778 eV 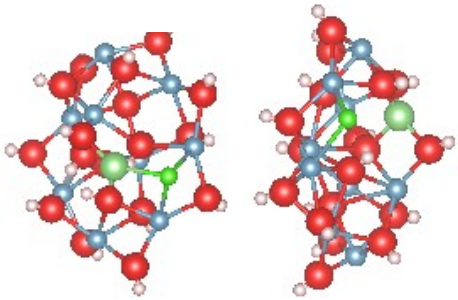 -198.622 eV -198.343 eV	
n=10	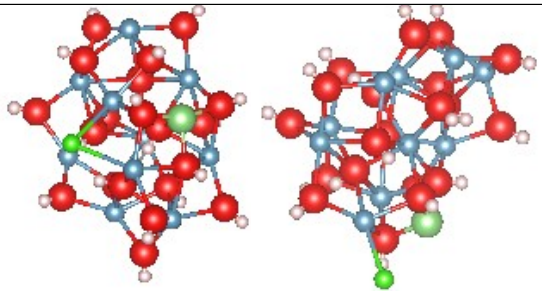 -221.007 eV -220.529 eV	

	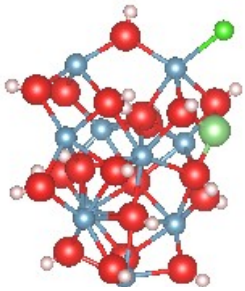 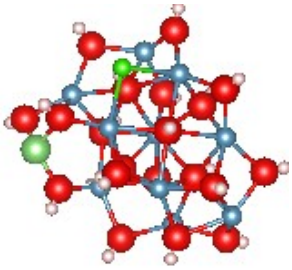 -220.479 eV -220.861 eV	
	LiOH- $(Ca(OH)_2)_n$	
n=1	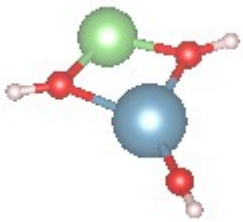 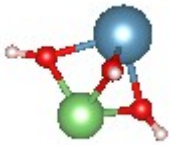 **-31.715 eV, -31.021 eV,** 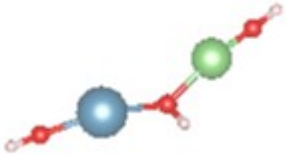 **-29.943 eV**	
n=2	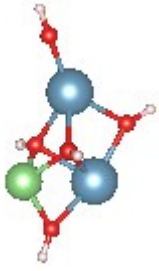 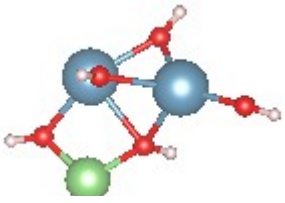 **-52.958 eV, -52.831 eV,**	

	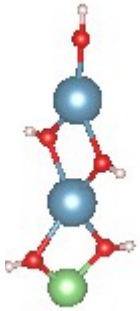 **-52.985 eV**	
n=3	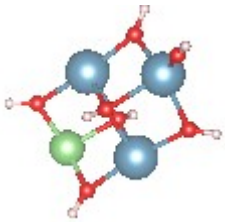  **-74.789 eV,** **-74.483 eV,** 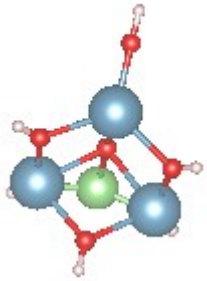 **-74.591 eV**	
n=4	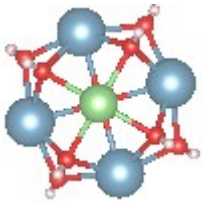 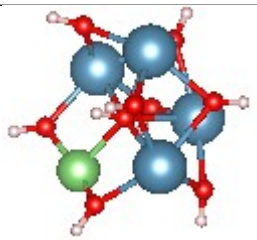 **-96.209 eV,** **-96.208 eV**	

	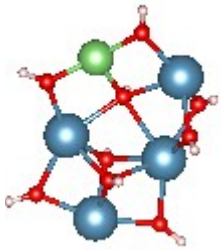 **-96.398 eV**	
n=5	 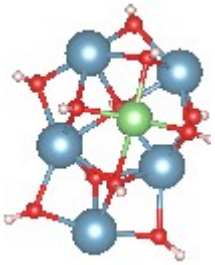 **-118.422 eV,** **-118.215 eV** 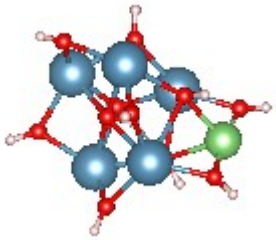 **-117.609 eV**	
n=6	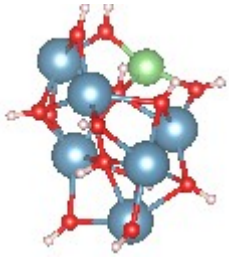 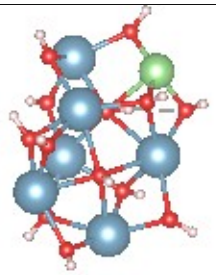 **-140.368 eV,** **-140.352 eV**	

	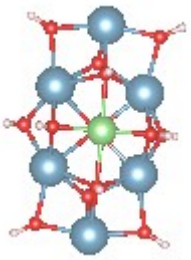 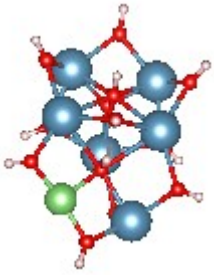 **-140.065 eV,** **-140.399 eV**	
n=7	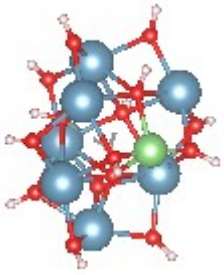 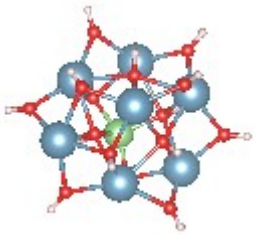 **-162.132 eV,** **-162.313 eV,** 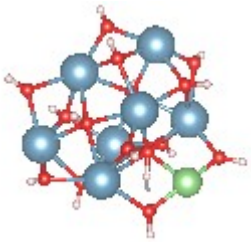 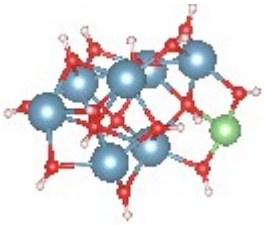 **-162.019 eV,** **-162.191 eV**	

n=8	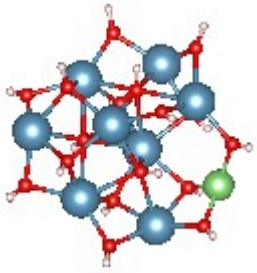 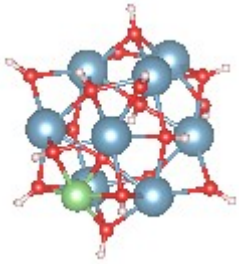 **-184.386 eV,** **-184.351 eV,** 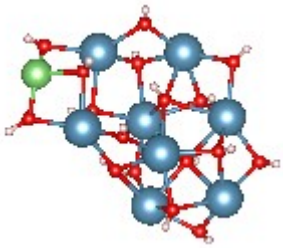 **-184.127 eV,**	
n=9	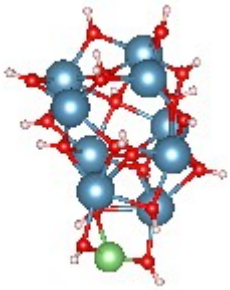 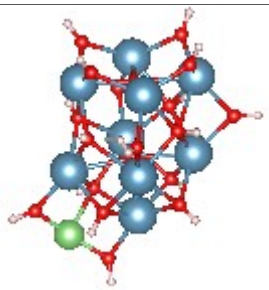 **-206.530 eV,** **-206.233 eV,** 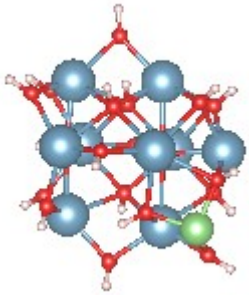 **-206.236 eV**	

n=10	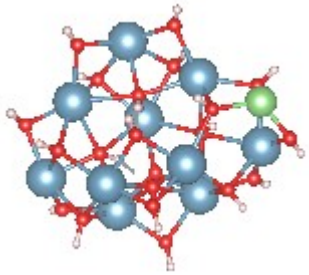 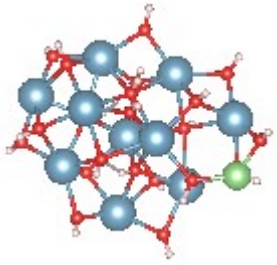 **-227.707 eV,** **-227.673 eV,** 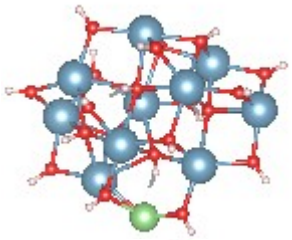 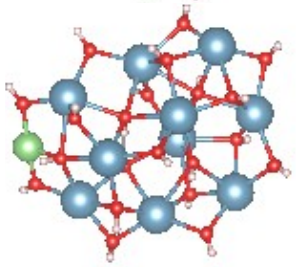 **-228.018 eV,** **-227.955 eV**	

APPENDIX 3 LiNO3, LiCl, and LiOH - [Ca(OH)2 low-lying isomers